

Decaying Neutrinos and Large Scale Structure Formation

Somnath Bharadwaj
Mehta Research Institute
Chhatnag Road, Jhusi
Allahabad 221 506
India
e-mail: somnath@mri.ernet.in

and

Shiv K. Sethi ¹
Inter-University Centre for Astronomy & Astrophysics
Post Bag 4
Pune 411007
India
e-mail: sethi@iucaa.ernet.in

ABSTRACT

We study the growth of density perturbations in a universe with unstable dark matter particles. The mass (m_ν) range $30 \text{ eV} \leq m_\nu \leq 10 \text{ keV}$ with lifetimes (t_d) in the range $10^7 \text{ sec} \leq t_d \leq 10^{16} \text{ sec}$ are considered. We calculate the COBE normalized matter power spectrum for these models. We find that it is possible to construct models consistent with observations for masses $m_\nu > 50 \text{ eV}$ by adjusting t_d so as to keep the quantity $m_\nu^2(\text{keV})t_d(\text{yr})$ constant at a value around 100. For $m_\nu \leq 1 \text{ keV}$ the power spectrum has extra power at small scales which could result in an early epoch of galaxy formation. We do not find any value of t_d which gives a viable model in the mass range $m_\nu \leq 50 \text{ eV}$. We also consider the implications of radiatively decaying neutrinos—models in which a small fraction $B \ll 1$ of neutrinos decay into photons—which could possibly ionize the intergalactic medium (IGM) at high redshift. We show that the parameter space of decaying particles which satisfies the IGM observations does not give viable models of structure formation.

Subject headings: large-scale structure of the universe—elementary particles:clustering—dark matter:intergalactic medium

¹Present address: Institut d'Astrophysique, 98 bis, boulevard Arago, 75014 Paris, France

1. Introduction.

To understand the formation of large scale structures in the universe is one of the most challenging problem in standard big bang cosmology. In recent years an overwhelming amount of evidence has accumulated which suggests that the formation of structures can be understood within the framework of the gravitational instability picture in which the structures form through the growth of small, scale-invariant, adiabatic perturbations created in the very early universe by some process like inflation (see Liddle & Lyth 1993 and references therein). The consistency of the CMBR anisotropies measured by the COBE-DMR (Smoot et al. 1992; Bennett et al. 1996)—which probe the matter fluctuations at recombination— with the present distribution of matter on large scales supports this view and suggests that the present universe is dominated by cold dark matter (CDM) particles. However the standard CDM model with $\Omega_0 = 1$, $h = .5$, and $n = 1$ normalized to COBE observations predicts neither the correct amplitude nor the correct shape of the power spectrum of density fluctuation at small scales (Efstathiou, Sutherland & Maddox 1990; Efstathiou, Bond, & White 1992; Peacock & Dodds 1994). The r.m.s. mass fluctuation in randomly placed spheres of radius $8h^{-1}$ Mpc (denoted by σ_8) provides a sensitive probe of the power spectrum at scales around $k = 0.2h$ Mpc $^{-1}$, and various studies show that the observed abundance of rich clusters of galaxies at the present epoch is consistent with $\sigma_8 \sim 0.5$ – 0.8 (Henry & Arnaud 1991; White et al. 1993; Viana & Liddle 1996; Bond & Myers 1996; Eke et al. 1996; Pen 1996; Borgani et al. 1997; Carlberg et al. 1997), whereas the standard CDM model normalized to the four-year COBE data predicts $\sigma_8 = 1.22$ (Bunn & White 1996). In addition, the standard CDM model is also inconsistent with the shape of the power spectrum inferred from various galaxy surveys (Baugh & Efstathiou 1994; Lin et al. 1996).

Within the framework of CDM-like models, the power spectrum of density fluctuation can be analyzed using a single parameter (Bardeen et al. 1986; Bond 1996)

$$\Gamma \simeq \Omega_{m0}h \times \left(\frac{\Omega_{r0}h^2}{4.18 \times 10^{-5}} \right)^{-1/2}. \quad (1)$$

Here $\Omega_{r0} = \rho_{r0}/\rho_{c0}$, where ρ_{r0} is the present energy density in all the relativistic species and ρ_{c0} is the present critical density, and Ω_{r0} is the contribution from the relativistic species to the present density parameter. Similarly, Ω_{m0} is the contribution to the present density parameter from the matter which can ‘effectively’ clump at small scales. While the standard CDM model predicts $\Gamma = 0.5$, observations require that $0.22 \leq \Gamma \leq 0.29$ (Peacock & Dodds 1994), and several variants of the standard CDM model have been proposed to overcome this discrepancy. There are essentially two ways to decrease Γ : 1. by decreasing the amount of matter which can clump at small scales (i.e., by decreasing Ω_{m0}) or 2. by increasing the radiation content of the universe. Models like λ CDM (Kofman et al. 1993; Liddle et al. 1996a; Stompor et al. 1995), HCDM (Klypin et al. 1993) and oCDM (Liddle et al. 1996b; Yamamoto & Bunn 1996) all involve a decrease in the value of Ω_{m0} . Models with decaying dark matter particle achieve the required

decrease in Γ by increasing Ω_{r0} (Bardeen, Bond, & Efstathiou 1987; Bond & Efstathiou 1991; White, Gelmini, & Silk 1995; McNally & Peacock 1996). In this paper we study the decaying neutrino model in some detail.

Decaying neutrinos models are characterized by two free parameters— m_ν , the mass of the decaying neutrino and t_d , the lifetime of the particle. In the early stages of the evolution when the temperature of the universe is much higher than m_ν , the energy density of the massive neutrinos is the same as the contribution from a massless species. As the universe expands the massive neutrinos become non-relativistic and the energy density in this component starts increasing relative to the contribution from the massless neutrinos. This gives rise to an era when the density of the universe is dominated by massive neutrinos, after which these particles decay and pump their rest energy into relativistic particles. Once the neutrinos decay the evolution of the universe is similar to the standard CDM model except that the energy density in relativistic particles is higher. This extra energy in the relativistic decay products gives the requisite increase in Ω_{r0} (Eq. 1) which acts to lower the value of Γ , and by suitably choosing m_ν and t_d it is possible to get results which are in agreement with the observed large scale structure.

Decaying neutrino models have been investigated by earlier authors (Bond & Efstathiou 1991; White, Gelmini, & Silk 1995) who find that at the length-scales which are relevant for large scale structure formation ($k \lesssim 0.1\text{Mpc}^{-1}$) the power spectrum is essentially of a CDM-like form with an effective Γ parameter which has a dependence on m_ν and t_d . This dependence captures the effect of the enhancement of Ω_{r0} , and in the mass range ($m_\nu \geq 1\text{keV}$) which they have considered this is the only process which affects the shape of the power spectrum in the relevant range of k . However, if one considers neutrinos with smaller masses and larger lifetimes, there are other physical processes which become important and the power spectrum starts to exhibit features which cannot be described by just changing the Γ for a CDM-like power spectrum. For large masses the viable models are restricted to have short lifetimes for otherwise the energy density of the decay product is too high and the resultant value of Γ turns out to be too low. In such models the massive neutrino dominated era ends much before any of the relevant length-scales enter the horizon. For low neutrino masses the viable models require larger lifetimes, and for many such models the size of the horizon in the massive neutrino dominated era is comparable to the length-scales which are relevant for large scale structure formation. The main effect on the power spectrum is that the modes which enter the horizon in the massive neutrino dominated era have more power compared to a CDM-like power spectrum and a CDM-like fit based on adjusting Γ does not work for these models.

In this paper we study in some detail the power spectrum for a large class of decaying neutrino models in the mass range $30\text{eV} \leq m_\nu \leq 10\text{keV}$. In addition to the large masses considered in earlier works (Bond & Efstathiou 1991; White, Gelmini, & Silk 1995) we have also considered models with low masses and large lifetimes, the upper limit on the lifetime coming from the restriction that the massive neutrino has to decay before the present epoch. We have not considered models where the massive neutrinos survive until the present epoch. While for large

masses the free-streaming of the massive neutrinos has no effect on large scale structure formation, this process has to be taken into account when dealing with neutrinos with low masses and large lifetimes. Sub-horizon scale perturbations in relativistic collision-less particles are wiped out due to the free-streaming of the particles. The massive neutrinos behave like relativistic particles as long as their momentum is much larger than the rest mass, and sub-horizon scale perturbations in the massive neutrino component start growing only after the particles become non-relativistic. The earlier works dealt with the perturbations in the massive neutrino component using the hydrodynamic equations which cannot capture the effects of free-streaming, and hence they were restricted to large masses. In this paper we have used the collision-less Boltzmann equation which allows us to follow the free-streaming of the massive neutrinos and hence we have been able to study models with low masses and long lifetimes. For a detailed discussion of free-streaming the readers is referred to Bond & Szalay (1983). The relevant equations for following the growth of perturbations in a decaying massive neutrino scenario are presented in the Appendix.

The power spectrum for the various decaying neutrino models have been normalized so that the theoretically predicted CMBR anisotropies are consistent with the COBE-DMR observations. For some of the decaying neutrino models the normalization differs significantly from the standard CDM model and this happens because of a large contribution from the ‘integrated Sachs-Wolfe effect’. For a discussion of the ‘integrated Sachs-Wolfe effect’ (Sachs & Wolfe 1967) in the context of some other large scale structure formation models the reader is referred to Kofman & Starobinsky (1985) and Sugiyama & Gouda (1992).

The motivation for studying cosmological models with decaying massive neutrinos has been twofold. As discussed earlier, decaying neutrinos provide possible scenarios for large scale structure formation. Decaying neutrinos are also interesting in the context of another very important problem in cosmology— to understand the ionization of the intergalactic medium (IGM) at high redshifts (Sciama 1990; Sethi 1997). The ionization state of the IGM at high redshifts is inferred from Gunn-Peterson tests for neutral hydrogen, neutral helium, and singly ionized helium, and also the proximity effect (see eg. Miralda-Escudé & Ostriker 1990; Giroux and Shapiro 1996; Sethi & Nath 1996), and it is not clear if the conventional sources of photoionization can serve the purpose of ionizing the IGM. Radiatively decaying neutrino models where a small fraction $B \ll 1$ of neutrinos decay into photons have been proposed as a possible means of photoionizing the IGM (Sethi 1997). In this paper we have investigated if any of the radiatively decaying neutrino models which can explain the ionization state of the IGM can also predict a large scale structure formation scenario which is compatible with observations.

For the radiatively decaying neutrinos, in addition to the two parameters m_ν and t_d , the branching ratio for decay into photons B is another free parameter. However, since $B \ll 1$ this affects only the ionization state of the IGM. The decay photons are dynamically unimportant and they do not affect the evolution of the dark matter perturbations. Thus, for the purpose of calculating the matter power spectrum we need consider only m_ν and t_d as the relevant parameters and the value of B is of no consequence.

From the point of view of particle physics models, we require: (1) $t_d \ll t_0$, t_0 being the present age of the universe and (2) for radiatively decaying neutrinos, radiative lifetime ($= t_d/B$) such that the intergalactic medium can be ionized. The latter was studied in Sethi (1997) and such models are possible within the framework of left-right symmetric models or models involving a charged Higgs scalar (see Fukugita and Yanagida 1995 for a recent review). To satisfy the first condition, we need to construct models where all the neutrinos have decayed by the present epoch. One of the models in which it can be implemented is a non-minimal Majoran model. In this model the dominant decay mode of the neutrino is a massless neutrino and a Majoran, and it is easy to get $10^7 < t_d < 10^{16}$ sec for $10 \text{ keV} > m_\nu > 100 \text{ eV}$ (Gelmini, Nussinov & Peccei 1992). The models we study are quite distinct from another class of radiatively decaying neutrino models suggested to solve several galactic and extragalactic observations by Sciama (1990). The dominant mode of decay in Sciama’s neutrinos is radiative with radiative lifetimes of $\sim 10^{23}$ sec with masses $m_\nu \simeq 30 \text{ eV}$. As these neutrinos are essentially stable over the age of the universe, structure formation with these neutrinos closely resembles HDM models (for more details see Sciama 1994) and they are not considered here.

Finally, we briefly outline the organization of the paper. In Section 2. we qualitatively discuss the physical effects that decide the power spectrum in a decaying neutrino model. The detailed equations and the computational method we use to numerically calculate the power spectrum are presented in the Appendix. Section 3. contains the results of our computations. We analyze the general features of the power spectrum for different decaying neutrino models and viable models are chosen on the basis of comparison to observations. In section 4. we present the summary and a discussion of the results. Appendix A contains the equations which govern the evolution of perturbations in the metric and in the various constituents of a decaying neutrino model. We work in the synchronous gauge and in our analysis we treat only the scalar perturbations. Appendix B contains a discussion of the initial conditions that we have used for the perturbations. Appendix C contains the equations which we have used to calculate the CMBR anisotropy and normalize the power spectrum. In Appendix D we briefly describe the scheme that we have used to numerically compute the power spectrum.

2. Physical effects in the decaying neutrino model.

In this section we qualitatively discuss some of the physical processes which shape the power spectrum in a decaying neutrino model, The detailed equations are presented in the Appendix.

The first ingredient in any such model is the power spectrum of initial perturbations on scales larger than the horizon. Here we assume that the initial perturbations have been produced by some viable model of inflation and we use a scale invariant Harrison-Zel’dovich power spectrum of the form $P_i(k) = Ak$. As the universe evolves the horizon expands, and the shape of the power

spectrum on sub-horizon scales gets modified by various astrophysical processes. The evolution of the power spectrum in the linear regime is expressed using the transfer function $T(k)$ which relates the final power spectrum $P_f(k)$ to the initial power spectrum i.e. $P_f(k) = T(k)P_i(k)$. Below we discuss the various physical processes that decide the shape of the matter transfer function in a universe with decaying neutrinos.

In all the models that we have studied CDM particles are the most dominant component of the present universe and it is the evolution of perturbations in this component which is of primary interest. The CDM perturbations are coupled to the other constituents of the universe through the gravitational potential which at any epoch is largely due to the most dominant component of the universe at that epoch. So we first discuss which of the various components dominates the universe in the different stages of its expansion and later discuss how this decides the shape of the transfer function.

In a spatially flat universe the evolution of the scale factor is governed by the equation

$$\frac{d}{d\eta}a(\eta) = \sqrt{\frac{8\pi G}{3}\rho(\eta)a^4(\eta)} = H_0\sqrt{\omega(\eta)}. \quad (2)$$

where $\eta(t) = \int_0^t (1/a(t')) dt'$ is the conformal time and $H_0 (= 100h \text{ km/s/Mpc})$ is the present value of the Hubble parameter, $\rho(\eta)$ is the total energy density of the universe (for decaying neutrino models it is contributed by the photons, 2 massless neutrinos, CDM particles, massive neutrinos, and neutrino decay product) and $\omega(\eta) = \rho(\eta)a^4(\eta)/\rho_{c0}$, where ρ_{c0} is the present value of the critical density. The variable $\omega(\eta)$ has been chosen so that at present it coincides with the value of the density parameter $\Omega_0 = 1$.

We first consider a universe with only two kinds of constituents 1. relativistic particles (referred to as radiation) which at present contribute Ω_{r0} to the density parameter, and 2. pressureless massive particles (referred to as matter) which at present contribute Ω_{m0} to the density parameter. The radiation make a constant contribution $\omega_r(\eta) = \Omega_{r0}$ while the contribution from matter $\omega_m(\eta) = a(\eta)\Omega_{m0}$ increases as the universe expands, and the universe proceeds from a radiation dominated era to a matter dominated era as it expands. The transition between the two regimes occurs when the matter and radiation make equal contributions to $\omega(\eta)$, and the value of the conformal time at the epoch of matter-radiation equality is given by

$$\eta_{\text{eq}} = 2(\sqrt{2} - 1) \frac{\sqrt{\Omega_{r0}}}{\Omega_{m0}H_0}. \quad (3)$$

In the radiation dominated era the Jeans length is of the order of the horizon ($\sim c\eta$), and perturbations in all components grow (i.e. $\delta(k, \eta) \propto \eta^2$, where the mode $k = 2\pi/\lambda$) when they are on scales larger than the horizon (i.e. they satisfy $kc\eta \ll 1$). The growth stops if the modes enter the horizon (i.e. $k \sim \pi/(c\eta)$) in the radiation dominated era. Once the universe gets matter dominated, matter perturbations on all scales grow in the same way ($\delta(k, \eta) \propto \eta^2$). Using $k_{\text{eq}} = \pi/(c\eta_{\text{eq}})$ to denote the mode which enters the horizon at the epoch of matter-radiation

equality, we can say that all modes with $k < k_{\text{eq}}$ entered the horizon in the matter dominated era and they all grow by the same factor during the course of the evolution. The modes with $k > k_{\text{eq}}$ enter the horizon in the radiation dominated era and as a consequence they experience a period of stagnation when they don't grow and the amplitude of these perturbations is suppressed by the factor $(k_{\text{eq}}/k)^2$ relative to the modes which enter in the matter dominated era. This fact can be used to crudely model the transfer function using the simple form $T(k) = 1$ for $k < k_{\text{eq}}$ and $T(k) = (k_{\text{eq}}/k)^4$ for $k \geq k_{\text{eq}}$, and it depends on just one quantity—the mode which enters the horizon at the epoch of matter radiation equality

$$k_{\text{eq}} = \frac{\pi}{2(\sqrt{2}-1)} \frac{\Omega_{m0}}{\sqrt{\Omega_{r0}}} \frac{H_0}{c}. \quad (4)$$

In the standard CDM model Ω_{r0} ($= 4.18 \times 10^{-5} h^{-2}$) has contributions from the CMBR photons and 3 massless neutrino species, and the matter, which is largely made up of CDM particles has $\Omega_{m0} = \Omega_{\text{CDM}0} = 1$, and we have $k_{\text{eq}} = 0.2 h^2 \text{Mpc}^{-1}$. It should be noted that here, and in the rest of the paper, we have ignored the dynamical effect of the baryon density Ω_{B0} .

The decaying neutrino model has all the ingredients of the standard CDM model the only difference being that one of the three neutrinos is massive. For neutrino masses $m_\nu < 1 \text{ MeV}$ the massive neutrinos decouple when they are relativistic, and after this the comoving number density of the neutrinos remains fixed, and at present we expect to find around 112.5 neutrinos/cm⁻³ (for the present temperature of CMBR $T_0 = 2.73 \text{ K}$). Once the temperature of the neutrinos falls below m_ν the massive neutrinos become nonrelativistic and they contribute to the matter density, and, if the neutrinos remain stable up to the present epoch, this contribution at present will be $\Omega_{m\nu 0} = m_\nu / (93.6 h^2 \text{ eV})$. So at any epoch before the massive neutrinos decay we have $\omega_r(\eta) = 3.62 \times 10^{-5} h^{-2}$ (from the photons and two massless neutrinos) and $\omega_m(\eta) = a(\eta)(\Omega_{\text{CDM}0} + \Omega_{m\nu 0}) = a(\eta)(1 + \Omega_{m\nu 0})$, and the epoch of matter radiation equality is at $t_{\text{eq}1}$ with

$$\eta_{\text{eq}1} = 2(\sqrt{2}-1) \frac{\sqrt{\Omega_{r0}}}{(1 + \Omega_{m\nu 0}) H_0}. \quad (5)$$

The universe remains matter dominated from the epoch $t_{\text{eq}1}$ to t_d when the massive neutrinos decay into 2 massless particles referred to as the relativistic decay product. When the massive neutrino decays, the matter density falls from $\omega_m(\eta) = a(\eta)(1 + \Omega_{m\nu 0})$ to $\omega_m(\eta) = a(\eta)$, and the rest energy of the massive neutrinos gets converted into radiation. This causes $\omega_r(\eta)$ to increase from Ω_{r0} to $\Omega_{r0} + a_d \Omega_{m\nu 0}$ (where $a_d = a(t_d)$) and the universe becomes radiation dominated for a second time. The second radiation dominated era starts at

$$\eta_d = \frac{1}{H_0} \left[\frac{12 t_d H_0}{(1 + \Omega_{m\nu 0})} \right]^{1/3} \quad (6)$$

when

$$a_d = \frac{(1 + \Omega_{m\nu 0})^{1/3}}{4} [12 t_d H_0]^{2/3} \quad (7)$$

and after this the evolution is just like the standard CDM model except that in this case the radiation density is higher. The universe has a second epoch of matter-radiation equality at

$$\eta_{\text{eq}2} = 2(\sqrt{2} - 1) \frac{\sqrt{\Omega_{r0} + a_d \Omega_{m\nu 0}}}{H_0}. \quad (8)$$

and after this the universe is dominated by the CDM particles. The shape of the transfer function is determined by the modes which are entering the horizon at the epochs when the universe changes from radiation to matter dominated and vice-versa. Expressing these in terms of the corresponding mode in the standard CDM model (i.e. $k_{\text{eq}} = 0.2h^2 \text{ Mpc}^{-1}$), we have

$$k_{\text{eq}1} = 1.07(1 + \Omega_{m\nu 0})k_{\text{eq}}, \quad (9)$$

$$k_d = \left[\frac{3.97 \times 10^9 \text{ sec}}{t_d} (1 + \Omega_{m\nu 0}) \right]^{1/3} h^{-4/3} k_{\text{eq}}, \quad (10)$$

$$(11)$$

and

$$k_{\text{eq}2} = k_{\text{eq}} \times \left[0.866 + \left(\frac{t_d}{5.59 \times 10^{10} \text{ sec}} \right)^{2/3} (1 + \Omega_{m\nu 0})^{1/3} \Omega_{m\nu 0} h^{8/3} \right]^{-1/2}. \quad (12)$$

For the modes which enter the horizon after the neutrinos decay the transfer function is of the same form as the standard CDM transfer function with $T(k) = 1$ for $k < k_{\text{eq}2}$, and $T(k) = (k_{\text{eq}2}/k)^4$ for $(k_{\text{eq}2} \leq k < k_d)$. Also, as $k_{\text{eq}2} < k_{\text{eq}}$, the power is reduced on larger scales as compared to the CDM model.

All the modes which enter the horizon in the first matter dominated era grow by the same factor and they experience a period of stagnation when the universe is radiation dominated for the second time. The amplitude of these modes is suppressed by the factor $(\eta_d/\eta_{\text{eq}2})^2$ relative to the modes which enter in the final matter dominated era, and the transfer function has the form $T(k) = (k_{\text{eq}2}/k_d)^4$ in the range $(k_d \leq k < k_{\text{eq}1})$. The modes which enter the horizon in the first radiation dominated era experience a further period of stagnation corresponding to the interval between their entering horizon and $\eta_{\text{eq}1}$ when the universe becomes matter dominated for the first time, and for $k \geq k_{\text{eq}1}$ the transfer function has the form $T(k) = (k_{\text{eq}2}/k_d)^4 (k_{\text{eq}1}/k)^4$.

In figure 1 we show the contribution to $\omega(\eta)$ from the various species for a universe with $h = 0.5$, and a decaying neutrino with $m_\nu = 200 \text{ eV}$ and $t_d = 10^{13} \text{ s}$. In this figure the contribution to $\omega(\eta)$ from the different constituents is plotted against the mode $k = \pi/c\eta$ which is entering the horizon at that epoch. This illustrates how the dominant component changes and which are the modes inside the horizon as these changes occur.

In figure 2 we show the transfer function for this decaying neutrino model based on the simple considerations discussed above. In the same figure we have also shown the results of a more detailed numerical computation of the transfer function for the same decaying neutrino model. In the latter calculation we have numerically followed the evolution of both the metric, and the

relevant properties of the different constituents. For the background universe we have solved for the scale factor along with the density of the different constituents. For the massive neutrinos we have used the distribution function to calculate the background density and this accurately follows the evolution of these particles from the relativistic to the nonrelativistic regime. This also takes into account the fact that relativistic time dilation causes the faster moving neutrinos to live longer in the frame of the cosmological observer.

We have calculated the evolution of the metric perturbations in the synchronous gauge and we have dealt with only the scalar part of the perturbations. For the CDM perturbations we have used the pressureless hydrodynamic equations. We have treated the photon-baryon fluid in the tightly coupled limit and we have ignored the baryon density in studying the dynamics. For the massless neutrinos, the massive neutrinos and the relativistic decay product we have used the collisionless Boltzmann equation to follow the evolution of perturbations of the distribution function, and we have used this to calculate the perturbation in the density, pressure and the anisotropic stresses. This takes into account the fact that the relativistic neutrinos have a very large mean free path (of the size of the horizon) and all sub-horizon perturbations in this component are wiped out due to the free-streaming of these neutrinos. Sub-horizon perturbations in the massive neutrino component grow only after the neutrino becomes nonrelativistic. The evolution of perturbations in the other components affects the CDM perturbations only through the metric perturbation and the Appendix contains a more detailed description of the equations we have used to follow the evolution of the perturbations.

In figure 2 we also show the numerically computed transfer function for the standard CDM model with $h = 0.5$. We see that the main effect of the decaying neutrinos is to reduce power on all scales except on a small range of scales near the first matter radiation equality $k_{\text{eq}1}$.

We have normalized the power spectrum for the decaying neutrino models by calculating the r.m.s. quadrupole moment Q_{rms} of the angular distribution of the temperature fluctuation in the CMBR, and we have normalized the power spectrum to $Q_{\text{rms}} = 17\mu\text{K}$. This is consistent with data from four years of COBE-DMR observations (Bunn & White 1996). On large angular scales ($\theta > 1^\circ$) the major contribution to the anisotropy in the CMBR is due to the linear Sachs-Wolfe effect (Sachs & Wolfe, 1967) which is an integral of the η derivative of the metric perturbations along the photon's trajectory from the last scattering surface to us. In the standard CDM model the photons decouple from the baryons in the matter dominated era, and this integral is restricted to the matter dominated era and it can be reduced to a surface term which relates the anisotropy in the CMBR to the fluctuations in the gravitational potential at the last scattering surface. In the decaying neutrino models we have two radiation dominated era, and there may be significant contributions to the CMBR anisotropies from the metric perturbations in the second radiation dominated era. For these models it is not possible to analytically calculate the CMBR anisotropy, and we have numerically evaluated the integral over the metric perturbations to calculate the CMBR anisotropy. We have used this to normalize the power spectrum for all the decaying neutrino models and the details are presented in the Appendix.

The normalization is significantly different from the standard CDM model in only those cases where the second matter-radiation equality occurs quite late i.e. ($\eta_{\text{eq}2} \sim \eta_0$, where η_0 is the value of the conformal time at present). The extreme case of such a situation is where the universe remains radiation dominated until the present epoch and such cases can be ruled out from age constraints. If the universe remained radiation dominated until the present epoch, the age of the universe would be $1/2H_0^{-1}$ as compared to $2/3H_0^{-1}$ for the matter dominated case, and an age as short as $\sim 10^{10}$ Gyr is ruled out by the observations of the oldest globular clusters. We have only considered those models where the universe is matter dominated at present. As we shall see in the next section, there are models which satisfy this criterion but still have a significant contribution from the ‘Integrated Sachs-Wolfe effect,’ and the normalization of the power spectrum for these models is quite different from the standard CDM normalization.

It is possible to think of the HCDM models as a limiting case of a decaying neutrino model with a small neutrino mass and $t_d \gg t_0$, however, there is a qualitative difference between the HCDM models and the decaying neutrino models. For the decaying neutrino models the constraint that the age of the universe is required to be $\simeq 2/3H_0^{-1}$ implies that the energy in the form of the relativistic decay products must be negligible at present, and the universe is largely dominated by the CDM particles ($\Omega_{\text{CDM}} \sim 1$) which clump at small scales. This should be contrasted with the the HCDM models where 20–30% of the matter at present is in the form of low mass neutrinos which do not clump at small scales.

3. Results

In this section we analyze the numerically computed power spectrum for a large class of decaying neutrino models and we compare our results with observations at various length scales.

Allowed models are selected on the basis of comparison to:

1. the observed cluster abundance (which probes scales $\simeq 8h^{-1}$ Mpc) (White et. al 1993; Eke et. al 1996; Henry & Arnaud 1991; Viana & Liddle 1996; Bond & Myers 1996; Pen 1996; Borgani et al. 1997; Carlberg et al. 1997),
2. the peculiar velocity measurements on scales up to $60h^{-1}$ Mpc (Bertschinger et al. 1990; Courteau et al. 1993; for comprehensive reviews see Strauss & Willick 1995; Dekel 1994 and references therein),
3. the three-dimensional power spectrum derived from the APM survey (Baugh & Efstathiou 1994), which determines the shape of the power spectrum on scales from $1h^{-1}$ Mpc to $50h^{-1}$ Mpc, and

4. the power spectrum obtained from the Las Campanas Redshift Survey (LCRS) (Lin et al. 1996).

We also compare the predictions of the allowed decaying neutrino models with the observed abundance of damped Lyman- α clouds at high redshifts.

3.1. Analysis of the linear power spectra.

For the scales which enter the horizon after the massive neutrinos decay (i.e. $k < k_d$), the massive neutrino model is akin to the standard CDM model, the only difference being the delay in the matter-radiation equality due to the additional radiation density contributed by the decay products. The delay in matter-radiation equality can be cast as a change in the ‘shape parameter’ $\Gamma = 5 k_{\text{eq}} h^{-1} \text{Mpc}$ for the power spectrum in CDM-like models, and for the decaying neutrino models we can similarly use $\Gamma = 5 k_{\text{eq}2} h^{-1} \text{Mpc}$, where $k_{\text{eq}2}$ can be calculated using equation (12). This definition of Γ is the same as the one used in equation (1) when the value of k_{eq} is expressed in terms of Ω_{r0} and Ω_{m0} . A point to note is that in the decaying neutrino models Γ depends on the parameters m_ν and t_d through the combination $t_d^2(1 + m_\nu/(93.6h^2 \text{eV}))m_\nu^3$ (eq. 12). and there is a degeneracy in the relation between m_ν , t_d and Γ . In the limit $m_\nu \gg 93.6h^2 \text{eV}$ this relation is simpler and we find Γ depends on just the combination $m_\nu^2 t_d$, which is in agreement with White, Gelmini, & Silk (1995), and contrary to the $m_\nu t_d$ scaling obtained by Bond & Efstathiou (1991).

A comparison of various numerically computed power spectra with the fit using $\Gamma = 5 k_{\text{eq}2} h^{-1} \text{Mpc}$ shows that for large masses this slightly underestimates the value of Γ , and we obtain a better fit using a minor variant of the form for Γ proposed by White, Gelmini, & Silk (1995).

We find that for large masses $m_\nu \gtrsim 1 \text{keV}$ and small lifetimes $t_d \leq 100\text{yr}$, the power spectrum in the range $k < 1h^{-1} \text{Mpc}^{-1}$ is well described by a CDM-like power spectrum

$$P(k) = Ak \times \left[1 + (ak + (bk)^{3/2} + (ck)^2)^\nu \right]^{-2/\nu}, \quad (13)$$

with $a = (6.4/\Gamma)h^{-1} \text{Mpc}$, $b = (3/\Gamma)h^{-1} \text{Mpc}$, and $c = (1.7/\Gamma)h^{-1} \text{Mpc}$. where our best fit Γ is:

$$\Gamma \simeq h \times \left(1 + 0.15 \left[\left(\frac{m_\nu}{1 \text{keV}} \right)^2 \frac{t_d}{1 \text{yr}} \right]^{2/3} \right)^{-1/2}, \quad (14)$$

which differs from the fit given by White, Gelmini, and Silk (1995) only in a small change of the numerical coefficient. The value of normalization A is determined from COBE observations and may contain a substantial contribution from the ‘integrated Sachs-Wolfe’ effect (Section (2) and Appendix C). For these decaying neutrino models ($m_\nu \gtrsim 1 \text{keV}$ and $t_d \leq 100\text{yr}$) a pure CDM-like fitting function correctly describes the linear power spectrum for the purposes

of comparing the theoretical predictions with observations like peculiar velocities of galaxies, galaxy-galaxy correlation functions and cluster abundances which probe the power spectrum at scales $k < 1h\text{Mpc}^{-1}$. At smaller scales ($k > 1h\text{Mpc}^{-1}$) these models start exhibiting an enhancement of power due to the matter dominated era caused by the massive neutrinos before they decay, and a CDM-like fit is inappropriate.

For smaller neutrino masses $m_\nu < 1\text{keV}$ and long lifetimes $t_d \gg 100\text{yr}$, the mode k_d enters the range $k \leq 1h\text{Mpc}^{-1}$ and a CDM-like fit is not adequate to describe all the features of the power spectrum at these length-scales. We find that a CDM-like form correctly describes the initial deviation (at $k \sim k_{eq2}$) of the power spectrum from the primordial Harrison Zel'dovich form, but it fails on scales $\sim k_d$ where there is a significant enhancement of power in the decaying neutrino models. The enhancement of power is most pronounced at the scales $k_d \lesssim k \lesssim k_{eq1}$ which entered the horizon when the universe was dominated by the massive neutrinos. The scales $k > k_{eq1}$ entered the horizon during the era when the massive neutrino was relativistic and the universe was experiencing the first radiation dominated phase. The growth of perturbations on these scales is suppressed due to free-streaming of the neutrinos and the oscillations in the photon-baryon fluid.

In figure 3 we show several power spectra for different decaying neutrino models with $h = 0.5$, and m_ν and t_d such that for all of them the product $m_\nu^2 t_d$ has the constant value which, according to equation (14), corresponds to $\Gamma \simeq 0.24$. In the range $k \leq 5h\text{Mpc}^{-1}$ the curve for $m_\nu = 10\text{keV}$ is indistinguishable from a CDM-like spectrum with $\Gamma = .24$. As m_ν is reduced the power spectrum starts deviating from the pure CDM-like form and it starts exhibiting the various small scale features mentioned above and discussed in detail in section 2. The change in small scale power in the linear power spectrum can be quantified using σ_R which is the theoretically predicted r.m.s. mass fluctuation in randomly placed spheres of radius $Rh^{-1}\text{Mpc}$. It should be noted that the σ_R discussed here is calculated using linear theory and for scales smaller than $R = 8$ non-linear effects have to be taken into account before this can be compared with observations. The change in small scale power as the neutrino mass is decreased is shown for various length-scales in figure 4, the largest scale being $8h^{-1}\text{Mpc}$ where the mass fluctuation is observationally very well determined and the smallest being $.25h^{-1}\text{Mpc}$ which is comparable to the scales important for the formation of damped Lyman- α clouds discussed later in this section. We find that as the mass is decreased there is nearly a two-fold increase in the small scale power compared to what one expect from a pure $\Gamma = .24$ CDM spectrum. At the scale $8h^{-1}\text{Mpc}$ the mass fluctuation keeps on increasing monotonically as m_ν is reduced and this results in some of the low mass models predicting too high a value of σ_8 to be compatible with observations. At smaller scales $\lesssim 2h^{-1}\text{Mpc}$ the mass fluctuation initially increases as m_ν is reduced but then starts decreasing again. This happens because for low neutrino masses these scales enter the horizon before the massive neutrinos become non-relativistic and the growth of fluctuations at these scales is suppressed.

Figure 3 also shows the APM power spectrum with a bias parameter $b = 1.2$. Also shown is the best fit to LCRS power spectrum (Eq. 23 in Lin et al.'s paper) with $b = 1.2$. While there are uncertainties in the value of the bias parameter for the galaxy surveys, it is believed that the value

of σ_8 as determined from cluster abundances is relatively free of bias. We have chosen the value $b = 1.2$ for the APM survey to make the observed power spectrum compatible with $\sigma_8 = 0.55$, and we have used this to visually compare the shape of observed power spectrum with the theoretically predicted power spectra for various decaying neutrino models. For comparison we have also shown the $\Gamma = 0.5$ CDM power spectrum which is obtained in the standard CDM model with $h = 0.5$. While we have shown the linear power spectrum for the various theoretical models, the observationally determined power spectrum has significant non-linear effects at $k > 0.2h\text{Mpc}^{-1}$ and a detailed comparison is not possible at these scales until these effects have been taken into account.

We next briefly discuss the COBE normalization of the power spectrum for the different models. All the models shown in figure 3 have the same normalization which matches with the CDM normalization, and this happens because for all these models the second radiation dominated era ends much before the present epoch i.e. ($\eta_{\text{eq}2} \sim .01\eta_0$). In figure 5 we show the power spectrum for the decaying neutrino model with $m_\nu = 100\text{eV}$, $t_d = 5 \times 10^{14}\text{sec}$ for which the second radiation dominated phase ends much later ($\eta_{\text{eq}2} \sim .1\eta_0$) and this corresponds to $\Gamma \sim .02$. We find that for this model the normalization is significantly lower than the CDM normalization due to the contribution from the ‘integrated Sachs-Wolfe effect’. We have considered a large number of different models where $\eta_{\text{eq}2} \sim .1\eta_0$, all of which satisfy the constraint that $t_0 \sim (2/3)H_0$ and we find that in all of them the effect is similar to the case shown in figure 5.

3.2. Allowed Models

A very sensitive observation for fixing the value of σ_8 is the abundance of rich clusters at the present epoch (Evrard 1989). Taking into account various uncertainties due to cluster temperatures, cluster x-ray luminosities, and the N-body methods in comparing theoretical estimates with observations fix the value of σ_8 between 0.5 and 0.9 (White et. al 1993; Eke et. al 1996; Henry & Arnaud 1991; Viana & Liddle 1996; Bond & Myers 1996; Pen 1996; Borgani et al. 1997; Carlberg et al. 1997). Larger values also seem to be ruled out by constraints from the pairwise random motions of galactic size dark matter halos (Gelb and Bertschinger 1994).

For a decaying neutrino model to be consistent with the galaxy surveys (APM, Baugh & Efstathiou 1994; LCRS, Lin et al. 1996) at large scales we have used the broad criterion that equation (14) should predict a value of Γ in the range $.2 \leq \Gamma \leq .3$ for the model, and we have discussed a set of models for which $\Gamma = .24$ in some detail.

In Table 1 we list the value of σ_8 for a wide range of decaying neutrino models. A class of models allowed by this observation is $m_\nu = 1\text{keV}$ and $t_d = 100\text{yr}$, and all the models obtained from this model keeping $m_\nu^2 t_d$ constant for $m_\nu > 50\text{eV}$ (figure 4), These models correspond to $\Gamma = 0.24$ at large scales. Not only do these models produce a value of σ_8 in the right range,

but as seen in figure 3, they also reproduce the shape of the observed galaxy power spectrum quite well. A comparison of the observed bulk velocities at scales ~ 40 Mpc and ~ 60 Mpc with the predictions of these models show that these models may not have enough large scale power (figure 6). However, due to systematic uncertainties in the analysis of the data and statistical uncertainties due to cosmic variance, the actual peculiar velocities can be much lower than the values shown in (figure 6) (Dekel 1994), and therefore a marginal inconsistency of our result with peculiar velocity measurements cannot rule out these models.

For the above class of models (i.e. $(m_\nu/1\text{keV})^2(t_d/1\text{yr}) = 100$) the value of σ_8 keeps on increasing as the mass is lowered below $\sim 200\text{eV}$ and the mass range $m_\nu \leq 50\text{eV}$ predicts too large a value of σ_8 to be compatible with observations of cluster abundances. Models with small masses ($m_\nu \leq 50\text{eV}$) are ruled out by the cluster abundance constraints irrespective of the value of t_d . We have run models for $m_\nu \leq 50\text{eV}$ with t_d varying over seven decades from 10^9 sec to 10^{16} sec and we do not find any for which $\sigma_8 \leq 0.9$. The upper limit on the value of t_d is chosen from the consideration of keeping the age of the universe $\sim 2/3H_0^{-1}$. The reason why it is not possible to get acceptable models in the low mass range is easy to understand. For the decay products to substantially delay the final matter radiation equality the massive neutrinos have to decay after they have become non-relativistic and they have a significant amount of rest energy to pump into the decay products. For this to happen these neutrinos should decay only after they have caused the universe to become matter dominated and remain matter dominated for some time. The epoch when the first matter radiation equality (η_{eq1}) occurs depends only on the mass of the neutrino (equation 5) and for masses $m_\nu \leq 50\text{eV}$ the mode k_{eq1} is very close to the mode $0.2h\text{Mpc}^{-1}$ which is the scale where the power spectrum is probed by σ_8 . As discussed in section 2, the power in the range of modes $k_{\text{eq1}} \geq k \geq k_d$ is enhanced as a consequence of the first matter dominated era, and this gives rise to a large value of σ_8 . Since k_{eq1} has no dependence on t_d , the value of σ_8 too is nearly independent of t_d for these models.

We find that by varying both m_ν and t_d it is possible to construct a large number of models all of which predict values of σ_8 which are in the correct range, and some of these are shown in Table 1 and figure 5. As one notices, models which give power spectra of very different shapes at larger scales can still produce acceptable values of σ_8 . However, most of these models have too small a power at large scales, and they do not predict a reasonable value for Γ . In addition, the peculiar velocities predicted by these models are too low to be consistent with observations (figure 6).

Going back to the allowed models, we find that an interesting region in the parameter space lies in the mass range $< 2\text{keV}$ which, apart from being in consonance with all the observations, can give extra power at small scales (figure 4; see also, McNally & Peacock 1996). This will result in an early epoch of galaxy formation which might ionize the hydrogen in the intergalactic medium, which is seen to be highly ionized up to $z \simeq 5$ (Giallongo et al. 1994). Recent observation of high redshift galaxies in the Hubble Deep Field (HDF) indicate that the number density of galaxies at $z \simeq 3$ may be comparable to the $z \simeq 0$ population (Steidel et al. 1996; Madau et al.

1996). Such observations require a high redshift of galaxy formation which occurs naturally within the framework of these decaying neutrino models.

Another possibility with the decaying neutrino scenario is to consider radiatively decaying neutrinos. In these models, a small fraction B of massive neutrinos decay into a photon and a massless neutrino. It is then possible to directly ionize the intergalactic medium at high redshifts by the decay photons (rather than by formation of high redshift objects). There exist a number of cosmological and astrophysical constraints on models of radiatively decaying neutrinos. These include constraints from the spectrum of the CMBR, the supernova 1987A, the cooling of red giants, and the diffuse extra-galactic background of photons, and for a detailed discussion of constraints on radiatively decaying neutrinos the reader is referred to Kolb & Turner (1990) and references therein. The parameter space for radiatively decaying neutrinos which is allowed by all these observations and which is consistent with the observed ionization state of the IGM had been studied by Sethi (1997). where it was shown that the acceptable values of B lie between 10^{-5} and 10^{-7} . For this range of B , the allowed values of t_d and m_ν lie between:

$$t_d \simeq 3 \times 10^{14} \text{sec} (m_\nu/100 \text{eV})^{-2.5} \quad (15)$$

and

$$t_d \simeq 3 \times 10^{15} \text{sec} (m_\nu/100 \text{eV})^{-2.5}. \quad (16)$$

We have calculated the power spectrum for several of the models allowed by the intergalactic medium ionization and in figure 7 we show some of the power spectra. The corresponding values of σ_8 and bulk velocities are shown in Table 1. It is clearly seen that all these model seem to be at variance with the observed galaxy power spectrum and peculiar velocity measurements. Figure 8 shows the approximate region of the $m_\nu - t_d$ parameter space allowed by the IGM constraints (Eq. (15) and (16)) as compared to the region of parameter space allowed by observations of the large scale structure in the universe, and it is clearly seen that there is no overlap between the two regions. For a given mass m_ν the lifetimes acceptable for large scale structure formation are too short as far as ionizing the IGM is concerned, and as seen in figure 8, these radiatively decaying models are ruled out by the shape of the observed power spectrum. However, it is worth mentioning that as noted in Sethi (1997), several of these models give acceptable value for σ_8 although they predict an unacceptable shape for the power spectrum. It should be mentioned that the gap between the ranges allowed by the structure formation and the IGM ionization is too large to be bridged by a change in cosmological parameters. However, the behaviour of the two allowed regions as cosmological parameters are varied can be qualitatively understood: for instance if the value of h is increased this would, for a given Ω_B , increase τ_{GP} because $\tau_{\text{GP}} \propto h^3$ (see e.g., Miralda-Escudé & Ostriker 1990), which means more ionizing photons would be required to satisfy the GP tests. If one keeps the value of B , the branching ratio, fixed, even larger values of $\{m_\nu, t_d\}$ are needed to ionize the IGM (Sethi 1997). An increase in the value of h would also mean more power at small scales (an increase in the value of Γ), which will have to be compensated by an increase in $\{m_\nu, t_d\}$. Therefore, the net results of an increase in the value of h would be to

shift up both the allowed regions in figure 8. Such an effect is difficult to quantify over an entire range of $\{m_\nu, t_d\}$ because of complicated dependence of the ionizing flux on m_ν and t_d .

3.3. High Redshift Objects.

The abundance of high redshift objects like damped Lyman- α clouds is an important diagnostic tool for studying structure formation models (Mo & Miralda Escudé 1994; Padmanabhan & Subramanian 1994). The neutral hydrogen column density of damped Lyman- α clouds is comparable to the present day spiral galaxies. Also the inferred sizes of these objects suggest that the damped Lyman- α clouds are progenitors of the present day spiral galaxies (Wolfe et al. 1992). Observations of damped Lyman- α clouds show that a large fraction of baryons in the form of neutral hydrogen may already have collapsed into forming these systems at $z \simeq 3$. According to Lanzetta, Wolfe, and Turnshek (1995) the quantity Ω_{HI} , which is the density of neutral hydrogen in damped Lyman- α clouds expressed as a fraction of the critical density, can be fit by a simple relation in the redshift range $z \simeq 0$ to $z \simeq 3$ (for $q_0 = 0.5$):

$$\Omega_{\text{HI}}(z) = 0.19 \pm 0.04 \times 10^{-3} h^{-1} \exp(0.83 \pm 0.15 \times z). \quad (17)$$

At higher redshift a decrease in Ω_{HI} has been reported (see for instance Storrie-Lombardi et al. 1995) which suggests that the formation of galaxies commenced around $z = 3$. For comparison with structure formation models one needs to know the mass of damped Lyman- α systems and this is highly uncertain. We follow Mo and Miralda-Escudé (1994) (see also McNally & Peacock 1996) in assuming that the minimum mass corresponding to these systems is $10^{9.6} h^{-1} M_\odot$ which corresponds to a virial velocity of $\sim 50 \text{ km sec}^{-1}$. This limit comes from the smallest halos which could cool sufficiently rapidly to collapse by $z \simeq 3$ (Efstathiou 1992). Knowing the minimum mass one can use the Press-Schechter formalism (Press & Schechter 1974) to calculate the fraction of the total matter which could collapse in forming structures with masses $\geq 10^{9.6} h^{-1} M_\odot$ at any redshift z . This can be multiplied with Ω_B to estimate the density of baryons that has collapsed into these objects and this gives

$$\Omega_{\text{col}}(M_{\text{min}}, z) = \Omega_B \times \left(1 - \text{erf} \left[\frac{\delta_c(1+z)}{\sqrt{(2)\sigma(M_{\text{min}}, 0)}} \right] \right) \quad (18)$$

The only input from structure formation models in equation (18) is the value of $\sigma(M_{\text{min}}, 0)$ which is the r.m.s. mass fluctuation in spheres of radius R ($\sim .3 \text{ Mpc}$) corresponding to M_{min} evaluated at the present epoch. The uppermost curve in figure 4 shows the value of σ_R at a comparable length-scale ($R = .25h \text{ Mpc}$) as a function of the neutrino mass for a class of allowed models, and this gives an idea of how this quantity changes for different decaying neutrino models. We also use $\delta_c = 1.686$ which is the value corresponding to the spherical collapse. It should be

pointed out that equation (18) gives the collapsed fraction of baryons in all the structures with masses $\geq M_{\min}$, though the masses of damped Lyman- α clouds lie between some M_{\min} and M_{\max} , which probably correspond to the virial velocity $\sim 200 \text{ km sec}^{-1}$, comparable to the present day galaxies. The collapsed fraction is extremely insensitive to the upper cut off in mass and changes negligibly as M_{\max} is changed from the mass corresponding to a virial velocity of $\sim 200 \text{ km sec}^{-1}$ to infinity which is the value that equation (18) assumes. This is expected because the probability of forming very high mass objects at high redshifts is exponentially suppressed.

An important point to note is that while Ω_{HI} in equation (17) refers to the neutral hydrogen observed in damped Lyman- α clouds, the quantity being calculated here i.e. Ω_{col} in equation (18) refers to the total amount of baryons that has collapsed into the damped Lyman- α clouds. It is expected that some of the collapsed baryons will be in the form of stars and ionized gas, and therefore any acceptable model of structure formation should predict a value for Ω_{col} which is at least equal to $\Omega_{HI}(z)$ if not larger.

In figure 9 we show the collapsed fraction Ω_{col} for some decaying neutrino models. While the baryon density was ignored when calculating the matter power spectrum for these models, we have used $\Omega_B = 0.05$ in equation (18). The shaded region in figure 9 shows the observed Ω_{HI} (Eq. (17)) for $h = 0.5$ and the data point at $z \simeq 4$ is taken from Storrie-Lombardi et al. 1995. For comparison we also show the collapsed fraction for a HCDM model with $\Omega_\nu = 0.25$, where Ω_ν is the fraction of the matter in the hot component. The power spectrum for the HCDM model was computed using COSMICS (Bertschinger & Bode 1995) with the value $\Omega_B = 0.05$. As is clearly seen the HCDM model seems to be at variance with observations as noted by several earlier authors (Mo & Miralda-Escudé 1994; Padmanabhan & Subramanian 1994; Ma & Bertschinger 1994; McNally & Peacock 1996; Ma et al. 1997; Gardner et al. 1997). The two decaying neutrino models considered here satisfy all the constraints discussed earlier in this section and the power spectra for these models is shown in figure 3. The collapsed fraction for both the models exceeds the observed $\Omega_{HI}(z)$ which indicates that both these models are compatible with the damped Lyman- α cloud observations. Similar conclusions are expected to hold for the other decaying neutrino models that pass the various tests discussed earlier this section. It should be pointed out that our computation of the matter power spectrum doesn't take into account the baryons. The inclusion of baryons reduces power at small scales (see e.g. Hu & Sugiyama 1996) which means that the computed fraction shown in figure 9 is an overestimate by 15–30 % depending on the value of Ω_B . However, it is evident from figure 9 that a decrement of this level in our computed Ω_{col} will not affect the conclusions of this comparison with observations of damped Lyman- α clouds..

Similar constraints on structure formation models can also be derived from the recent observation of high redshift galaxies (Steidel et al. 1996; Madau et al. 1996). However, there is an even greater uncertainty attached to the masses of these high redshift galaxies and comparison with structure formation models may not be so straight forward (Mo & Fukugita 1996) as for damped Lyman- α clouds.

4. Summary and Discussion

We have studied large scale structure formation in a $\Omega = 1$ universe with decaying massive neutrinos. This variant of the CDM model has two extra parameters— the neutrino mass m_ν and the lifetime of the massive neutrino t_d , and by varying these it is possible to introduce extra features into the power spectrum. We have computed the power spectrum for a large range of the parameters m_ν and t_d . Our analysis takes into account the free-streaming of the massive neutrinos, and this allows us to study a hitherto unexplored region of parameter space corresponding to low neutrino masses and large lifetimes.

Unlike other models of structure formation in the universe - for example the standard CDM model, and its variants like HCDM, λ CDM, ν CDM - the decaying neutrino model allows the possibility of introducing extra features in the power spectrum at both large scales ($k \leq 0.01 \text{ Mpc}^{-1}$) and small scales ($k \geq 0.1 \text{ Mpc}^{-1}$). The decay of the neutrino acts to reduce the power at large scales (as compared to CDM model) by increasing the radiation content of the universe to a value which can be much larger than what is obtained from three relativistic neutrino species. This reduces the power at large scales by delaying the matter radiation equality. In addition, the late radiation dominated era can affect the overall normalization of the power spectrum through the ‘integrated Sachs-Wolfe effect’ and we find that this can lead to an overall reduction of power at all scales. The decaying neutrino models also allow us the possibility of enhancing the power over a range of modes at small scales, and this is achieved by varying the parameters to suitably adjust the first era of matter radiation equality.

CDM-like models with Γ between 0.22 and 0.29 seem to be compatible with most observations (Peacock & Dodds 1994). To allow for the uncertainties in comparing the computed linear power spectra with the observed non-linear ones, i.e., from APM and LCRS surveys, we allow a larger range of Γ : $0.2 \leq \Gamma \leq 0.3$. We find that it is possible to construct a large number of models which predict a value of Γ in this range and the allowed region of parameter space is shown in figure 8. We have studied in some detail a class of models whose power spectrum is similar to a $\Gamma = .24$ CDM power spectrum at large scales near the turnaround from the primordial Harrison Zel’dovich form. We find that for the mass range $m_\nu \geq 10 \text{ keV}$, for the entire k range that we have studied (i.e. $k \leq 5h \text{ Mpc}^{-1}$), the power spectrum is indistinguishable from a CDM power spectrum with $\Gamma \simeq 0.24$. As the mass is reduced below 10 keV the power spectrum starts getting extra power at small scales and the shape of the power spectrum starts to differ considerably from a CDM-like power spectrum with a Γ fit. We find that the models in the mass range $m_\nu > 50 \text{ eV}$ are roughly consistent with the APM and LCRS power spectrum, and with σ_8 inferred from cluster abundances, but with extra power at small scales. We find that the predicted r.m.s. peculiar velocities in spheres of radius $40h^{-1} \text{ Mpc}$ and $60h^{-1} \text{ Mpc}$ are somewhat below those indicated by observations, but the discrepancy is not as severe so as to conclusively rule out these models. For masses $\leq 50 \text{ eV}$ the values predicted for σ_8 are too large to be compatible with observations of cluster abundances. This conclusion is independent of the choice of t_d and we fail to find any value

of t_d for which models with $m_\nu \leq 50\text{eV}$ produces an acceptable power spectrum.

We also find that for very small masses the neutrinos have to decay very late if this process is to have a significant effect on the power spectrum. In these models the power spectrum has too much power at small scales and too little power at large scales, and these models are ruled out by observations (figures 3, 5 and 7, and Table 1).

We have compared the predictions of some of the allowed decaying neutrino models with the observations of the abundances of damped Lyman- α clouds at high redshifts and we find that the decaying neutrino models are compatible with these observations.

We have addressed the question if any of the radiatively decaying neutrino models which can reionize the intergalactic medium is consistent with the observed large scale structure of the universe. We fail to find any model which can reionize the IGM and also produce an acceptable power spectrum in a $\Omega = 1$ universe. It is still to be seen if such models can be constructed by considering open universes or by introducing a cosmological constant. In addition to the constraints on radiatively decaying neutrinos considered in this paper, models which predict very early reionization are also constrained by CMBR observations at small angular scales (Netterfield et al. 1997). However, as we find that these models are ruled out by the structure formation considerations presented in this paper, we have not considered the small angle CMBR observations here. Incidentally, an early epoch of enhanced galaxy formation may be expected in the allowed models with extra small scale power, and this may provide a method of reionizing the IGM. Issues related to galaxy formation in a decaying neutrino model are beyond the scope of this paper, and they require a more detailed analysis involving N-body simulations and baryonic physics. Such an analysis will also be able to put further restrictions on the allowed regions of the $m_\nu-t_d$ parameter space. In addition, N-body simulations for the decaying neutrino power spectra will permit comparison with the observed power spectrum at scales where the non-linear effects are important and this can be used to put restrictions on the allowed models.

Finally, although we see that it is possible to use the observed distribution of matter in the universe to restrict the parameter space of decaying neutrino models, it seems implausible that these observation will be able to distinguish a decaying neutrino model from other variants of the CDM model in the near future. However, the study of CMBR anisotropies at small angular scales holds the promise of being able to discriminate between these models and possibly single out the correct one. Two satellite projects planned for the next decade —MAP and Planck surveyor (COBRAS-SAMBA)—will map the CMBR sky at a few arc-minutes angular resolutions, and it is hoped that these observations will unambiguously validate one of the models and reject the rest. In light of this it important to understand the small angular scale anisotropies in the CMBR for the various allowed decaying neutrino models, and work is in progress in this direction.

The authors would like to thank Tarun Souradeep for useful discussions. S.B. would like to thank Rajaram Nityananda for some useful discussions, and the Raman Research Institute for the

use of its computer facility in the early stages of this project. S.K.S. would like to thank Profs. J. R. Bond and J. Silk for useful comments and suggestions. The authors thank the referee Martin White for useful comments and suggestions.

A. Formalism

Here we briefly discuss the equations that govern the evolution of the scale factor and linear perturbations in a spatially flat universe which is composed of CDM particles, photons tightly coupled to baryons, massless neutrinos and massive neutrinos which have the possibility of decaying into some massless (relativistic) decay products. The evolution of both the background universe and the perturbations is governed by the Einstein equations

$$R_{\nu}^{\mu} = 8\pi G(T_{\nu}^{\mu} - \frac{1}{2}\delta_{\nu}^{\mu}T). \quad (\text{A1})$$

where the Ricci tensor R_{ν}^{μ} is calculated from the metric, and the energy momentum tensor T_{ν}^{μ} has contributions from all the different particle species. In this part of the paper we use $c = 1$.

In the synchronous gauge the metric components can be written as

$$g_{00} = -a^2(\eta) \quad g_{0i} = 0 \quad g_{ij} = a^2(\eta) [\delta_{ij} + h_{ij}(\mathbf{x}, \eta)] \quad (\text{A2})$$

where the zeroth component of the coordinates refers to the conformal time η and h_{ij} is the metric perturbation. Using this in the Einstein equation one obtains the equation for the scale factor and the metric perturbation. Using prime to denote derivative with respect to η , the equation for the scale factor can be written as

$$a'(\eta) = H_0 \sqrt{\omega(\eta)}. \quad (\text{A3})$$

This equation is discussed in some detail in section 2. We next consider the equations for the evolution of h_j^i the metric perturbation. We proceed by first calculating the perturbation in the Ricci tensor caused by the metric perturbation. We only use the components R_0^0 and R_j^0 , and keeping only terms linear in h_j^i , we obtain

$$\Delta R_0^0 = \frac{1}{2a^2} \left(h'' + \frac{a'}{a} h' \right) \quad (\text{A4})$$

and

$$\Delta R_j^0 = \frac{1}{2a^2} \left(h'_{,j} - h'_{j,l} \right). \quad (\text{A5})$$

Here h is the trace of the metric perturbation, and we have used the notation $_{,j} \equiv \frac{\partial}{\partial x^j}$.

It is possible to decompose the metric perturbation into scalar, vector and tensor components, and at the linear order these evolve independently. Retaining only the scalar parts, we write the metric perturbation as

$$h_j^i(\mathbf{x}, \eta) = \int \frac{d^3k}{(2\pi)^3} e^{i\mathbf{k}\cdot\mathbf{x}} \frac{1}{3} \left[\mu(\mathbf{k}, \eta) \delta_j^i + \lambda(\mathbf{k}, \eta) \left(\delta_j^i - 3 \frac{k^i k_j}{k^2} \right) \right] \quad (\text{A6})$$

where μ which is the Fourier transform of h corresponds to isotropic dilations or contractions, and λ , which is the traceless part, corresponds to shear. Expressing the Fourier transform of the curvature in terms of these quantities we have

$$\Delta \tilde{R}_0^0(\mathbf{k}, \eta) = \frac{1}{2a^2} \left(\mu'' + \frac{a'}{a} \mu' \right) \quad (\text{A7})$$

and

$$\Delta \tilde{R}_j^0(\mathbf{k}, \eta) = \frac{ik_j}{3a^2} (\mu' + \lambda') \quad (\text{A8})$$

We also write the Fourier transform of the linear order perturbation to the energy momentum tensor as

$$\Delta \tilde{T}_0^0(\mathbf{k}, \eta) = -\Delta \rho(\mathbf{k}, \eta) \quad \Delta \tilde{T}_j^i(\mathbf{k}, \eta) = \Delta P(\mathbf{k}, \eta) \delta_j^i + \frac{1}{2} \Delta Q(\mathbf{k}, \eta) \left(\delta_j^i - 3 \frac{k^i k_j}{k^2} \right). \quad (\text{A9})$$

where $\Delta \rho(\mathbf{k}, \eta)$, $\Delta P(\mathbf{k}, \eta)$ and $\Delta Q(\mathbf{k}, \eta)$ are the Fourier transform of the perturbations in the density, the pressure and the anisotropic stresses respectively. The perturbations to the components T_j^0 also have contributions at linear order, but as discussed below, the final equations that we use do not have any explicit reference to $\Delta \tilde{T}_j^0$.

Using the above expressions in the Einstein equation, the 0_0 component gives us an equation for μ

$$\mu'' + \frac{a'}{a} \mu' = -3H_0^2 a^2 \left(\frac{\Delta \rho}{\rho_{c0}} + 3 \frac{\Delta P}{\rho_{c0}} \right). \quad (\text{A10})$$

To follow the evolution of λ we use the 0_j component of the Einstein equation which gives us

$$\mu' + \lambda' = \frac{-9H_0^2 a^2}{\rho_{c0}} \frac{ik^j}{k^2} \Delta \tilde{T}_j^0. \quad (\text{A11})$$

Differentiating this once with respect to η and using the energy-momentum conservation equation $T_{j;\mu}^\mu = 0$, we obtain the following equation for λ

$$\lambda'' + \frac{a'}{a} (2\lambda' + \mu') = 3H_0^2 a^2 \left(\frac{\Delta \rho}{\rho_{c0}} + 3 \frac{\Delta Q}{\rho_{c0}} \right). \quad (\text{A12})$$

Finally, we have the equations (A3), (A10) and (A12) which we use to follow the evolution of a, μ and λ respectively. The right hand side of these equations has quantities which refer to the

total density, pressure and anisotropic stresses. These have contributions from the different species of particles and we have to consider them separately. The total effect is obtained by summing over the contribution from the different species e.g. $\omega = \sum \omega_{species}, \Delta\rho = \sum \Delta\rho_{species}$, etc. In the following subsections we separately consider the different kinds of species we have taken into account.

A.1. The ideal fluids.

Cold dark matter particles and photons which are tightly coupled to baryons can be treated as ideal fluids. The energy momentum tensor then has the form

$$T_{\nu}^{\mu} = P\delta_{\nu}^{\mu} + (P + \rho)U^{\mu}U_{\nu} \quad (\text{A13})$$

where $U^{\mu}(x, \eta)$ is the bulk 4 velocity of the fluid, and there are no anisotropic stresses i.e. $Q = 0$.

The CDM particles can be considered as dust for which there is no pressure i.e. $P_{\text{CDM}} = 0$. We choose a synchronous coordinate system which moves with the dust particles and hence these particles have no peculiar velocities i.e. $U_{\text{CDM}}^{\mu} = (1/a, 0, 0, 0)$. The energy-momentum conservation equation $T_{\text{CDM} 0;\mu}^{\mu}$ for the CDM component then gives the equation

$$\omega_{\text{CDM}}(\eta) = a(\eta)\Omega_{\text{CDM}0} \quad (\text{A14})$$

for the background density, and the equation

$$\delta'_{\text{CDM}}(\mathbf{k}, \eta) + \frac{1}{2}\mu'(\mathbf{k}, \eta) = 0 \quad (\text{A15})$$

with

$$\frac{\Delta\rho_{\text{CDM}}}{\rho_{c0}} = \frac{\omega_{\text{CDM}}\delta_{\text{CDM}}}{a^4},$$

for the density perturbation.

The photon-baryon fluid has the equation of state $P_{\gamma} = (1/3)\rho_{\gamma}$. For this fluid the energy momentum conservation equations give the equation

$$\omega_{\gamma}(\eta) = \Omega_{\gamma 0} \quad (\text{A16})$$

for the background density. Perturbations in this medium produce bulk flows relative to the synchronous coordinate system, and in addition to the perturbation in the density, one has to also consider the perturbation to the velocity of the fluid $\Delta U_{\gamma}^i(x, \eta)$. Only the divergence of this quantity ($\theta_{\gamma} = \Delta U_{\gamma,i}^i$) couples to the density perturbation, and the energy-momentum conservation gives us the equations

$$\delta'_{\gamma}(\mathbf{k}, \eta) + \frac{4}{3}\tilde{\theta}_{\gamma}(\mathbf{k}, \eta) + \frac{2}{3}\mu'(\mathbf{k}, \eta) = 0 \quad (\text{A17})$$

and

$$\tilde{\theta}'_\gamma(\mathbf{k}, \eta) - \frac{k^2}{4}\delta_\gamma(\mathbf{k}, \eta) = 0 \quad (\text{A18})$$

which we use to follow the evolution of $\Delta\rho_\gamma/\rho_{c0} = \omega_\gamma\delta_\gamma/a^4$ and $\Delta P_\gamma/\rho_{c0} = \omega_\gamma\delta_\gamma/(3a^4)$.

A.2. Neutrinos.

It is not possible to treat neutrinos as a perfect fluid and a microscopic description is required. Every particle is fully described by its position in space-time and its momentum. Instead of using the momentum components in the synchronous coordinate system, it is more convenient to use the components of the momentum on the tetrad

$$\mathbf{e}_b = \frac{1}{a^2}(\delta_b^\mu - \frac{1}{2}h_b^\mu)\frac{\partial}{\partial x^\mu} \quad \mathbf{e}^b = a^2(\delta_\mu^b + \frac{1}{2}h_\mu^b)dx^\mu \quad (\text{A19})$$

introduced by Bond & Szalay (1983). Here the tetrad index b takes values 0, 1, 2, 3, and the tetrad is orthogonal (but not normal). The metric has components $g_{bc} = \mathbf{g}(\mathbf{e}_b, \mathbf{e}_c) = a^{-2}\eta_{bc}$ on the tetrad, and a particle's 4-momentum \mathbf{p} has components $\mathbf{p} = q^a\mathbf{e}_a$ on the tetrad. The components q^a are related by $q^a q^b \eta_{ab} = -a^2 m^2$, and any 3 of the 4 components are sufficient to fully describe the momentum state of a particle. We use the 3 spatial components q^i and the zeroth component is obtained from these using $q^0 = \sqrt{q^2 + a^2 m^2}$, where q^2 is used to denote $\delta_{ij}q^i q^j$.

Next, the equation of motion (parallel transport) $\nabla_{\mathbf{p}}\mathbf{p} = 0$ for a particle is used to arrive at the equation for the evolution of q^a

$$q^b \mathbf{e}_b(q^a) = - [(\nabla_{\mathbf{e}_b} \mathbf{e}_c)(\mathbf{e}^a)] q^b q^c. \quad (\text{A20})$$

Keeping only terms linear in the metric perturbation equation (A20) gives

$$q^b \mathbf{e}_b(q^i) = -\frac{1}{2a^2} q^b q^c (h_{b,c}^i - h_{bc,}^i) \quad (\text{A21})$$

for the spatial components of the momentum q^i , and it follows that in the absence of any perturbations the 3 spatial components of the momentum remain constant, and they evolve only due to the perturbation in the metric.

The state of a large number of neutrinos of a particular species can be described by a distribution function $f(\mathbf{x}, \mathbf{q}, \eta)$ which is the number density of these particles in phase space, and its evolution equation

$$q^a \mathbf{e}_a(f) + q^a \mathbf{e}_a(q^i) \frac{\partial}{\partial q^i} f = 0 \quad (\text{A22})$$

follows from the local conservation of particles in phase space. We also consider situations where the particles of a particular species decay to produce particles of a different species, and for such

situations it is necessary to introduce a source term in equation (A22). This is discussed later in this section.

The distribution function is next decomposed into two parts, an isotropic function of q corresponding to the distribution of particles in the unperturbed universe, and another corresponding to the perturbation i.e.

$$f(\mathbf{x}, \mathbf{q}, \eta) = \bar{f}(q, \eta) + \delta f(\mathbf{x}, \mathbf{q}, \eta). \quad (\text{A23})$$

Equation (A22) then gives

$$\frac{\partial}{\partial \eta} \bar{f}(q, \eta) = 0 \quad \text{i.e.} \quad \bar{f}(q, \eta) = \bar{f}(q) \quad (\text{A24})$$

for the unperturbed distribution function. For neutrinos the unperturbed distribution function is the Fermi-Dirac distribution function

$$\bar{f}_\nu(q) = \frac{2}{h_P^3 [\exp(q/k_B T_{\nu 0}) + 1]} \quad (\text{A25})$$

where the factor 2 takes into account the fact that for every neutrino species there will be both particles and anti-particles, h_P is the Planck constant, k_B is the Boltzmann constant and $T_{\nu 0} = 2.726^\circ K/1.4$ is the present temperature of the relic cosmic neutrinos.

For the perturbation, equation (A22) gives us

$$\frac{\partial}{\partial \eta} \delta f + \frac{q^i}{q^0} \delta f_{,i} - \frac{q^i q^j}{2q} h'_{ij} \frac{\partial}{\partial q} \bar{f} = 0. \quad (\text{A26})$$

Using $F(\mathbf{k}, \mathbf{q}, \eta)$ to denote the Fourier transform of $\delta f(\mathbf{x}, \mathbf{q}, \eta)$ and using α to denote the cosine of the angle between \mathbf{q} and \mathbf{k} , equation (A26) can be written as

$$\frac{\partial}{\partial \eta} F + \frac{i\alpha q k}{q^0} F - \frac{q}{6} [\mu' + (1 - 3\alpha^2)\lambda'] \frac{\partial}{\partial q} \bar{f} = 0. \quad (\text{A27})$$

and we use these equations to follow the evolution of the energy momentum tensor

$$T_b^a = \frac{\eta_{bc}}{a^4} \int \frac{q^a q^c}{q^0} f d^3 q. \quad (\text{A28})$$

The background density can be written in terms of the distribution function as

$$\rho(\eta) = \frac{1}{a^4} \int q^0 \bar{f}(q, \eta) d^3 q, \quad (\text{A29})$$

and the various perturbed quantities that appear in the equation for μ and λ can be written as

$$\Delta \rho(\mathbf{k}, \eta) = \frac{1}{a^4} \int q^0 F(\mathbf{k}, \mathbf{q}, \eta) d^3 q, \quad (\text{A30})$$

$$\Delta P(\mathbf{k}, \eta) = \frac{1}{3a^4} \int \frac{q^2}{q^0} F(\mathbf{k}, \mathbf{q}, \eta) d^3 q \quad (\text{A31})$$

and

$$\Delta Q(\mathbf{k}, \eta) = \frac{1}{3a^4} \int (1 - 3\alpha^2) \frac{q^2}{q^0} F(\mathbf{k}, \mathbf{q}, \eta) d^3 q. \quad (\text{A32})$$

A.2.1. *Massless neutrinos.*

For massless neutrinos the calculation is greatly simplified because $q^0(q, \eta) = q$ which does not evolve in time. The integral in equation (A29) is a constant and as a result $\omega_\nu(\eta) = \Omega_{\nu 0}$. Equation (A27) is solved by the method of characteristics and the solution is

$$\begin{aligned} F_\nu(\mathbf{k}, \mathbf{q}, \eta) &= F_\nu(\mathbf{k}, \mathbf{q}, \eta_i) e^{-i\alpha k(\eta - \eta_i)} \\ &+ \frac{q}{6} \frac{\partial}{\partial q} \bar{f}_\nu \int_{\eta_i}^{\eta} \left[\mu'(\mathbf{k}, \tilde{\eta}) + (1 - 3\alpha^2) \lambda'(\mathbf{k}, \tilde{\eta}) \right] e^{-i\alpha k(\eta - \tilde{\eta})} d\tilde{\eta} \end{aligned} \quad (\text{A33})$$

where η_i is the instant when the initial conditions are specified and from which we start following the evolution of the perturbations. We use this in equations (A30), (A31) and (A32) where the d^3q integral can be done analytically. The angular integrals involve the following relation involving Legendre polynomials $P_l(x)$ and spherical Bessel functions $j_l(x)$

$$j_l(x) = \frac{i^l}{2} \int_{-1}^1 e^{i\alpha x} P_l(\alpha) d\alpha, \quad (\text{A34})$$

and for $l \geq 2$ we also define

$$\begin{aligned} \mathcal{F}_l(x) &= \frac{1}{8l^3 + 12l^2 - 2l - 3} \left[(6l^3 + 15l^2 + 3l - 6) j_{l+2}(x) - (4l^3 + 6l^2 + 2l) j_l(x) \right. \\ &+ \left. (6l^3 + 3l^2 - 9l) j_{l-2}(x) \right] = \frac{i^l}{2} \int_{-1}^1 e^{i\alpha x} (1 - 3\alpha^2)^2 P_l(\alpha) d\alpha. \end{aligned} \quad (\text{A35})$$

We use these to obtain

$$\begin{aligned} \frac{\Delta\rho_\nu(\mathbf{k}, \eta)}{\rho_{c0}} &= 3 \frac{\Delta P_\nu(\mathbf{k}, \eta)}{\rho_{c0}} = -\frac{2\omega_\nu}{3a^4} \left\{ [\mu(\mathbf{k}, \eta_i) j_0(k(\eta - \eta_i)) + 2\lambda(\mathbf{k}, \eta_i) j_2(k(\eta - \eta_i))] \right. \\ &+ \left. \int_{\eta_i}^{\eta} \left[\mu'(\mathbf{k}, \tilde{\eta}) j_0(k(\eta - \tilde{\eta})) + 2\lambda'(\mathbf{k}, \tilde{\eta}) j_2(k(\eta - \tilde{\eta})) \right] d\tilde{\eta} \right\} \end{aligned} \quad (\text{A36})$$

and

$$\begin{aligned} \frac{\Delta Q_\nu(\mathbf{k}, \eta)}{\rho_{c0}} &= -\frac{4\omega_\nu}{3a^4} \left\{ [\mu(\mathbf{k}, \eta_i) j_2(k(\eta - \eta_i)) + \lambda(\mathbf{k}, \eta_i) \mathcal{F}_2(k(\eta - \eta_i))] \right. \\ &+ \left. \int_{\eta_i}^{\eta} \left[\mu'(\mathbf{k}, \tilde{\eta}) j_2(k(\eta - \tilde{\eta})) + \lambda'(\mathbf{k}, \tilde{\eta}) \mathcal{F}_2(k(\eta - \tilde{\eta})) \right] d\tilde{\eta} \right\}. \end{aligned} \quad (\text{A37})$$

It should be noted that in obtaining equations (A36) and (A37) we have used a particular form for the initial perturbation $F(\mathbf{k}, \mathbf{q}, \eta_i)$ which has been chosen such that it corresponds to the growing mode of the perturbation, and this is discussed in more detail later.

We use equation (A36) and (A37) to follow the evolution of perturbations in the massless neutrinos.

A.2.2. *Decaying massive neutrinos.*

For decaying massive neutrinos a source term has to be included in equation (A22) and we have

$$q^a \mathbf{e}_a(f_d) + q^a \mathbf{e}_a(q^i) \frac{\partial}{\partial q^i} f_d = -\frac{m_\nu}{t_d} f_d \quad (\text{A38})$$

where t_d is the lifetime of the massive neutrinos. The evolution of the unperturbed distribution function is governed by

$$\frac{q^0}{a^2} \frac{\partial}{\partial \eta} \bar{f}_d(q, \eta) = -\frac{m_\nu}{t_d} \bar{f}_d(q, \eta). \quad (\text{A39})$$

We write the solution of this equation in terms of the variable

$$\psi(q, \eta) = \int_{\eta_i}^{\eta} \frac{m_\nu a^2(\tilde{\eta})}{q^0(q, \tilde{\eta})} d\tilde{\eta}. \quad (\text{A40})$$

which corresponds to the proper time of a neutrino with spatial momentum q , and it goes over to the cosmological time t in the limit $q \ll am_\nu$. This variable takes into account the fact that the decay of the neutrino is governed by the passage of time in its own rest frame, and not in the frame of the cosmological observer. The solution for the unperturbed distribution function is

$$\bar{f}_d(q, \eta) = e^{-\psi(q, \eta)/t_d} \bar{f}_\nu(q). \quad (\text{A41})$$

where $\bar{f}_\nu(q)$ is the Fermi-Dirac distribution given in equation (A25). We use equation (A41) to follow the evolution of the background density of the massive neutrinos and we have

$$\rho_d(\eta) = \frac{1}{a^4} \int d^3q q^0(q, \eta) \bar{f}_d(q, \eta). \quad (\text{A42})$$

The equation for the perturbation is

$$\frac{\partial}{\partial \eta} \delta f_d + \frac{q^i}{q^0} \delta f_{d,i} - \frac{q^i q^j}{2q} h'_{ij} \frac{\partial}{\partial q} \bar{f}_d = -\frac{m_\nu a^2}{t_d q^0} \delta f_d \quad (\text{A43})$$

which can be simplified by defining

$$\delta f_d(\mathbf{x}, \mathbf{q}, \eta) = e^{-\psi/t_d} \delta \hat{f}_d(\mathbf{x}, \mathbf{q}, \eta) \quad (\text{A44})$$

and

$$\frac{\partial}{\partial q} \bar{g}_d(q, \eta) = \frac{\partial}{\partial q} \bar{f}_\nu(q) - \left[\frac{1}{t_d} \frac{\partial}{\partial q} \psi(q, \eta) \right] \bar{f}_\nu(q), \quad (\text{A45})$$

and equation (A43) can then be written as

$$\frac{\partial}{\partial \eta} \delta \hat{f}_d + \frac{q^i}{q^0} \delta \hat{f}_{d,i} - \frac{q^i q^j}{2q} h'_{ij} \frac{\partial}{\partial q} \bar{g}_d = 0. \quad (\text{A46})$$

Using $\hat{F}_d(\mathbf{k}, \mathbf{q}, \eta)$ to denote the Fourier transform of $\delta \hat{f}_d(\mathbf{x}, \mathbf{q}, \eta)$, the solution of equation (A46) can be written in Fourier space as

$$\begin{aligned} \hat{F}_d(\mathbf{k}, \mathbf{q}, \eta) &= \hat{F}_d(\mathbf{k}, \mathbf{q}, \eta_i) e^{-i\alpha k \tau} \\ &+ \frac{q}{6} \int_{\eta_i}^{\eta} \frac{\partial}{\partial q} \bar{g}_d(q, \tilde{\eta}) \left[\mu'(\mathbf{k}, \tilde{\eta}) + (1 - 3\alpha^2) \lambda'(\mathbf{k}, \tilde{\eta}) \right] e^{-i\alpha k(\tau - \tilde{\tau})} d\tilde{\eta} \end{aligned} \quad (\text{A47})$$

where the variable

$$\tau(q, \eta) = \int_{\eta_i}^{\eta} \frac{q}{q^0(q, \eta_1)} d\eta_1 \quad (\text{A48})$$

corresponds to the comoving distance a neutrino travels in the time interval $(\eta - \tilde{\eta})$, and we use $\tilde{\tau}$ to denote $\tau(q, \tilde{\eta})$. For massive neutrinos it is not possible to do the q integral analytically. Doing the angular integrals analytically we obtain

$$\begin{aligned} \Delta \rho_d(\mathbf{k}, \eta) &= \frac{2\pi}{3a^4} \int dq q^3 q^0 e^{-\psi/t_d} \left\{ \frac{\partial}{\partial q} \bar{f}_\nu(q) [\mu(\mathbf{k}, \eta_i) j_0(k\tau) + 2\lambda(\mathbf{k}, \eta_i) j_2(k\tau)] \right. \\ &+ \left. \int_{\eta_i}^{\eta} \frac{\partial}{\partial q} \bar{g}_d(q, \tilde{\eta}) \left[\mu'(\mathbf{k}, \tilde{\eta}) j_0(k(\tau - \tilde{\tau})) + 2\lambda'(\mathbf{k}, \tilde{\eta}) j_2(k(\tau - \tilde{\tau})) \right] d\tilde{\eta} \right\}, \end{aligned} \quad (\text{A49})$$

$$\begin{aligned} 3\Delta P_d(\mathbf{k}, \eta) &= \frac{2\pi}{3a^4} \int dq \frac{q^5}{q^0} e^{-\psi/t_d} \left\{ \frac{\partial}{\partial q} \bar{f}_\nu(q) [\mu(\mathbf{k}, \eta_i) j_0(k\tau) + 2\lambda(\mathbf{k}, \eta_i) j_2(k\tau)] \right. \\ &+ \left. \int_{\eta_i}^{\eta} \frac{\partial}{\partial q} \bar{g}_d(q, \tilde{\eta}) \left[\mu'(\mathbf{k}, \tilde{\eta}) j_0(k(\tau - \tilde{\tau})) + 2\lambda'(\mathbf{k}, \tilde{\eta}) j_2(k(\tau - \tilde{\tau})) \right] d\tilde{\eta} \right\}, \end{aligned} \quad (\text{A50})$$

and

$$\begin{aligned} 3\Delta Q_d(\mathbf{k}, \eta) &= \frac{4\pi}{3a^4} \int dq \frac{q^5}{q^0} e^{-\psi/t_d} \left\{ \frac{\partial}{\partial q} \bar{f}_\nu(q) [\mu(\mathbf{k}, \eta_i) j_2(k\tau) + \lambda(\mathbf{k}, \eta_i) \mathcal{F}_2(k\tau)] \right. \\ &+ \left. \int_{\eta_i}^{\eta} \frac{\partial}{\partial q} \bar{g}_d(q, \tilde{\eta}) \left[\mu'(\mathbf{k}, \tilde{\eta}) j_2(k(\tau - \tilde{\tau})) + \lambda'(\mathbf{k}, \tilde{\eta}) \mathcal{F}_2(k(\tau - \tilde{\tau})) \right] d\tilde{\eta} \right\}. \end{aligned} \quad (\text{A51})$$

We also use equation (A47) to follow the evolution of

$$\Delta n_d(\mathbf{k}, \eta) = \int F_d(\mathbf{k}, \mathbf{q}, \eta) d^3 q \quad (\text{A52})$$

and we obtain

$$\begin{aligned} \Delta n_d(\mathbf{k}, \eta) &= \frac{2\pi}{3} \int dq q^3 e^{-\psi/t_d} \left\{ \frac{\partial}{\partial q} \hat{f}_d(q) [\mu(\mathbf{k}, \eta_i) j_0(k\tau) + 2\lambda(\mathbf{k}, \eta_i) j_2(k\tau)] \right. \\ &+ \left. \int_{\eta_i}^{\eta} \frac{\partial}{\partial q} \bar{g}_d(q, \tilde{\eta}) \left[\mu'(\mathbf{k}, \tilde{\eta}) j_0(k(\tau - \tilde{\tau})) + 2\lambda'(\mathbf{k}, \tilde{\eta}) j_2(k(\tau - \tilde{\tau})) \right] d\tilde{\eta} \right\}, \end{aligned} \quad (\text{A53})$$

for this quantity which is relevant later for the study of perturbations in the decay product.

We use equations (A49), (A50) and (A51) to follow the evolution of perturbation in the massive decaying neutrinos.

A.2.3. *Decay product.*

Consider the decay of a massive neutrino which has momentum \mathbf{q} and hence is in motion relative to the observers who define the synchronous coordinate system. In its own rest frame the neutrino decays by emitting 2 massless particles in exactly opposite directions \mathbf{l} and $-\mathbf{l}$, and the direction \mathbf{l} is isotropically distributed. We use $\mathbf{Q}_1(\mathbf{q}, \mathbf{l})$ to denote the tetrad components of the momentum of the decay particle which was emitted in the direction \mathbf{l} in the neutrino's rest frame. Although the \mathbf{l} 's have an isotropic distribution, the $\mathbf{Q}_1(\mathbf{q}, \mathbf{l})$ s will not be isotropically distributed, and this happens because of the transformation from the the neutrino's rest frame to the tetrad. To avoid confusion with the phase space of the massive neutrino, we use coordinates $(\mathbf{x}, \mathbf{Q}, \eta)$ on the phase space of the decay product particles, and we add a source term to equation (A22) to follow the evolution of the decay products. This extra term takes into account the fact that massive neutrinos with all possible momenta \mathbf{q} decay in all possible directions \mathbf{l} (in the respective rest frame) to give rise to 2 decay product particles, and the equation for the evolution of the decay product is

$$Q^a \mathbf{e}_a(f_R(\mathbf{x}, \mathbf{Q}, \eta)) + Q^a \mathbf{e}_a(Q^i) \frac{\partial}{\partial Q^i} f_R(\mathbf{x}, \mathbf{Q}, \eta) = \frac{m_\nu}{t_d} \int d^3 q \frac{d\Omega_1}{4\pi} \delta^3(\mathbf{Q} - \mathbf{Q}_1(\mathbf{q}, \mathbf{l})) f_d(\mathbf{x}, \mathbf{q}, \eta). \quad (\text{A54})$$

For the unperturbed distribution function this gives us

$$Q \frac{\partial}{\partial \eta} \bar{f}_R(Q, \eta) = \frac{a^2 m_\nu}{t_d} \int d^3 q \frac{d\Omega_1}{4\pi} \delta^3(\mathbf{Q} - \mathbf{Q}_1(\mathbf{q}, \mathbf{l})) \bar{f}_d(q, \eta). \quad (\text{A55})$$

which on integrating over $d^3 Q$ gives

$$\frac{\partial}{\partial \eta} \omega_R(\eta) = \frac{a^2 m_\nu}{\rho_{c0} t_d} \int d^3 q \bar{f}_d(q, \eta) \quad (\text{A56})$$

for the background density of the decay product. For the perturbation we have

$$\begin{aligned} \frac{\partial}{\partial \eta} \delta f_R(\mathbf{x}, \mathbf{Q}, \eta) + \frac{Q^i}{Q} \delta f_{R,i}(\mathbf{x}, \mathbf{Q}, \eta) - \frac{Q^i Q^j}{2Q} h'_{ij} \frac{\partial}{\partial Q} \bar{f}_R(Q, \eta) = \\ \frac{a^2 m_\nu}{Qt_d} \int d^3 q \frac{d\Omega_1}{4\pi} \delta^3(\mathbf{Q} - \mathbf{Q}_1(\mathbf{q}, \mathbf{l})) \delta f_d(\mathbf{x}, \mathbf{q}, \eta). \end{aligned} \quad (\text{A57})$$

The initial condition for the decay product is different (i.e. $\delta f_R(\mathbf{x}, \mathbf{Q}, \eta) = 0$) as we assume that the initial density of the decay products is zero. Using this, the solution to equation (A57) can be written in Fourier space as

$$\begin{aligned} F_R(\mathbf{k}, \mathbf{Q}, \eta) &= \frac{Q}{6} \int_{\eta_i}^{\eta} \frac{\partial}{\partial Q} \bar{f}_R(Q, \tilde{\eta}) \left[\mu'(\mathbf{k}, \tilde{\eta}) + (1 - 3\alpha^2) \lambda'(\mathbf{k}, \tilde{\eta}) \right] e^{-i\alpha k(\eta - \tilde{\eta})} d\tilde{\eta} \\ &+ \frac{m_\nu}{Qt_d} \int d^3 q \frac{d\Omega_1}{4\pi} \delta^3(\mathbf{Q} - \mathbf{Q}_1(\mathbf{q}, \mathbf{l})) \int_{\eta_i}^{\eta} a^2(\tilde{\eta}) F_d(\mathbf{k}, \mathbf{q}, \tilde{\eta}) e^{-i\alpha k(\eta - \tilde{\eta})} d\tilde{\eta} \end{aligned} \quad (\text{A58})$$

where now α is the cosine of the angle between \mathbf{Q} and \mathbf{k} , and $F_d(\mathbf{k}, \mathbf{q}, \eta) = e^{-\psi/t_d} \hat{F}_d(\mathbf{k}, \mathbf{q}, \eta)$. We use this to calculate the density perturbation for which we obtain

$$\begin{aligned} \frac{\Delta\rho_R(\mathbf{k}, \eta)}{\rho_{c0}} &= 3 \frac{\Delta P_R(\mathbf{k}, \eta)}{\rho_{c0}} = -\frac{2\omega_R}{3a^4} \int_{\eta_i}^{\eta} \left[\mu'(\mathbf{k}, \tilde{\eta}) j_0(k(\eta - \tilde{\eta})) + 2\lambda'(\mathbf{k}, \tilde{\eta}) j_2(k(\eta - \tilde{\eta})) \right] d\tilde{\eta} \\ &+ \frac{m_\nu}{\rho_{c0} a^4 t_d} \int d^3q \frac{d\Omega_1}{4\pi} \int_{\eta_i}^{\eta} a^2(\tilde{\eta}) F_d(\mathbf{k}, \mathbf{q}, \tilde{\eta}) e^{-i\alpha_1(\mathbf{q}, \mathbf{l})k(\eta - \tilde{\eta})} d\tilde{\eta} \end{aligned} \quad (\text{A59})$$

where $\alpha_1(\mathbf{q}, \mathbf{l})$ is the cosine of the angle between $\mathbf{Q}_1(\mathbf{q}, \mathbf{l})$ and \mathbf{k} . Doing the integral keeping the \mathbf{q} and \mathbf{l} dependence of $\alpha_1(\mathbf{q}, \mathbf{l})$ is rather complicated. The calculation is greatly simplified if we assume that the neutrino is at rest when it decays. Under this assumption the angle α_1 is the cosine of the angle between \mathbf{l} and \mathbf{k} and it no longer depends on \mathbf{q} . This assumption is reasonably good in situations where the neutrino decays much after it has become nonrelativistic.

Under this assumption it is possible to analytically do the angular integral $d\Omega_1$, and we obtain

$$\begin{aligned} \frac{\Delta\rho_R(\mathbf{k}, \eta)}{\rho_{c0}} &= 3 \frac{\Delta P_R(\mathbf{k}, \eta)}{\rho_{c0}} = -\frac{2\omega_R}{3a^4} \int_{\eta_i}^{\eta} \left[\mu'(\mathbf{k}, \tilde{\eta}) j_0(k(\eta - \tilde{\eta})) + 2\lambda'(\mathbf{k}, \tilde{\eta}) j_2(k(\eta - \tilde{\eta})) \right] d\tilde{\eta} \\ &+ \frac{m_\nu}{\rho_{c0} a^4 t_d} \int_{\eta_i}^{\eta} a^2(\tilde{\eta}) j_0(k(\eta - \tilde{\eta})) \delta n_d(\mathbf{k}, \tilde{\eta}) d\tilde{\eta} \end{aligned} \quad (\text{A60})$$

and

$$\begin{aligned} \frac{\Delta Q_R(\mathbf{k}, \eta)}{\rho_{c0}} &= -\frac{4\omega_\nu}{3a^4} \int_{\eta_i}^{\eta} \left[\mu'(\mathbf{k}, \tilde{\eta}) j_2(k(\eta - \tilde{\eta})) + \lambda'(\mathbf{k}, \tilde{\eta}) \mathcal{F}_2(k(\eta - \tilde{\eta})) \right] d\tilde{\eta} \\ &+ \frac{2m_\nu}{\rho_{c0} a^4 t_d} \int_{\eta_i}^{\eta} a^2(\tilde{\eta}) j_2(k(\eta - \tilde{\eta})) \delta n_d(\mathbf{k}, \tilde{\eta}) d\tilde{\eta}. \end{aligned} \quad (\text{A61})$$

where

$$\delta n_d(\mathbf{k}, \eta) = \int F_d(\mathbf{k}, \mathbf{q}, \eta) d^3q.$$

The evolution of $\delta n_d(\mathbf{k}, \tilde{\eta})$ is governed by equation (A53) which has been obtained in the previous subsection. . We use equations (A60) and (A61) to follow the evolution of perturbations in the relativistic decay product.

B. Initial conditions.

Here we briefly discuss the initial conditions for adiabatic perturbations. The initial conditions are set at an early epoch when the universe is dominated by the relativistic particles i.e. photons

and neutrinos, and the massive neutrino behaves like a relativistic particle and can also be treated as a massless species. The scale factor then evolves as

$$a(\eta) = \eta H_0 \sqrt{\Omega_{\gamma 0} + (n_\nu + 1)\Omega_{\nu 0}} \quad (\text{B62})$$

where n_ν is the number of massless neutrino species, and $\Omega_{\nu 0}$ is the contribution that one massless neutrino species would make to the present value of Ω_0 . We also introduce the quantity

$$r_\nu = \frac{(n_\nu + 1)\Omega_{\nu 0}}{\Omega_{0\gamma} + (n_\nu + 1)\Omega_{\nu 0}} \quad (\text{B63})$$

which is the ratio of the density of the neutrinos to the total density of the universe in the radiation dominated era.

The initial epoch is also chosen such that all the relevant modes are outside the horizon i.e. $k\eta_i \ll 1$. In this limit the equations for the evolution of perturbations in the photons and the neutrinos are quite simple and can be analytically solved. In the limit $k\eta_i \ll 1$ the equation for the perturbation in the photon-baryon fluid becomes

$$\delta'_\gamma(\mathbf{k}, \eta) + \frac{2}{3}\mu'(\mathbf{k}, \eta) = 0. \quad (\text{B64})$$

For each neutrino species we define $\Delta\rho_\nu(\mathbf{k}, \eta) = 3\Delta P_\nu(\mathbf{k}, \eta) = \rho_\nu(\eta)\delta_\nu(\mathbf{k}, \eta)$ and $3\Delta Q_\nu(\mathbf{k}, \eta) = \rho_\nu(\eta)\Delta_\nu(\mathbf{k}, \eta)$, and in the limit $k\eta_i \ll 1$ equation (A27) gives us

$$\delta'_\nu(\mathbf{k}, \eta) + \frac{2}{3}\mu'(\mathbf{k}, \eta) = 0 \quad (\text{B65})$$

and

$$\Delta'_\nu(\mathbf{k}, \eta) + \frac{8}{15}\lambda'(\mathbf{k}, \eta) = 0. \quad (\text{B66})$$

We see that the evolution of both δ_γ and δ_ν are governed by the same equation and we can combine these two by defining

$$\delta = \frac{\omega_\gamma\delta_\gamma + (n_\nu + 1)\omega_\nu\delta_\nu}{\omega_\gamma + (n_\nu + 1)\omega_\nu}. \quad (\text{B67})$$

The photon-baryon fluid has no anisotropic stresses and there is no contribution from the photons to ΔQ .

We also have equations (A10) and (A12), which can now be written as

$$\mu'' + \frac{1}{\eta}\mu' = -\frac{6\delta}{\eta^2} \quad (\text{B68})$$

and

$$\lambda'' + \frac{1}{\eta}(2\lambda' + \mu') = \frac{3}{\eta^2}(\delta + r_\nu\Delta_\nu). \quad (\text{B69})$$

We simultaneously solve equations (B64), (B65), (B66), (B68) and (B69) to obtain the analytic form of the growing mode in the initial epoch, and the solution for the metric perturbation can be written as

$$\mu(\mathbf{k}, \eta) = \frac{\eta^2 C}{2} \quad \text{and} \quad \lambda(\mathbf{k}, \eta) = \frac{-10}{15 + 4r_\nu} \mu(\mathbf{k}, \eta) \quad (\text{B70})$$

where C is a constant which determines the amplitude of the perturbation at the initial epoch. Note that we solve for μ and λ only up to an additive constant, and since we only encounter the derivatives of μ and λ , the additive constant can be ignored for our purposes.

Using (B70) we can write the solution for the perturbation in the photon-baryon fluid as

$$\delta_\gamma(\mathbf{k}, \eta) = -\frac{\eta^2 C}{3} \quad \text{and} \quad \tilde{\theta}_\gamma(\mathbf{k}, \eta) = -\frac{\eta^3 k^2 C}{36}. \quad (\text{B71})$$

and for each neutrino species we can write the distribution function as

$$F_\nu(\mathbf{k}, \mathbf{q}, \eta) = \frac{q}{6} \left[\mu(\mathbf{k}, \eta) + (1 - 3\alpha^2) \lambda(\mathbf{k}, \eta) \right] \frac{\partial}{\partial q} \bar{f}_\nu. \quad (\text{B72})$$

The CDM particles do not contribute to the dynamics in the initial epoch, and they move like test particles to which our synchronous coordinate system is attached. We use equation (A15) to obtain

$$\delta_{\text{CDM}}(\mathbf{k}, \eta) = -\frac{1}{2} \mu(\mathbf{k}, \eta) \quad (\text{B73})$$

for the perturbation in the CDM component.

We use these solutions to fix the initial conditions at the epoch η_i . We also assume that there is no significant decay of the massive neutrino prior to the epoch η_i and we set the initial density of the decay product to zero.

C. CMBR anisotropies due to the Sachs-Wolfe effect.

At angular scales greater than a degree the dominant contribution to the anisotropies in the CMBR is largely due to the Sachs-Wolfe effect where the fluctuations in the CMBR temperature along any line of sight can be related to the derivative of the metric perturbation $h'_{a,b}(\mathbf{x}, \eta)$ integrated along the photons trajectory from the last scattering surface to the observer. For an observer located at \mathbf{x}_0 , the fluctuation in the CMBR temperature observed in the direction \mathbf{n} is given by

$$\frac{\Delta T}{T}(\mathbf{n}) = -\frac{1}{2} \int_{\eta_{\text{dec}}}^{\eta_0} h'_{ab}(\mathbf{x}_0 - \mathbf{n}\tilde{\eta}, \tilde{\eta}) n^a n^b d\tilde{\eta}. \quad (\text{C74})$$

where η_{dec} refers to the value of the conformal time at the epoch when the baryons and photons decouple, and η_0 is the present value of the conformal time.

The angular dependence of this temperature fluctuation can be expanded in terms of spherical harmonics $Y_l^m(\mathbf{n})$

$$\frac{\Delta T}{T}(\mathbf{n}) = \sum_{l,m} a_l^m Y_l^m(\mathbf{n}). \quad (\text{C75})$$

and the ensemble average of the square of the expansion coefficients gives the angular power spectrum

$$C_l = \langle |a_l^m|^2 \rangle \quad (\text{C76})$$

which, because the ensemble is statistically isotropic, has no m dependence. Writing the metric perturbation in terms of the Fourier expansion and using equation (C74) we write the CMBR angular power spectrum as

$$C_l = \frac{1}{4\pi} \int \frac{d^3k}{(2\pi)^3} |\Delta_l(\mathbf{k})|^2 \quad (\text{C77})$$

where

$$\Delta_l(\mathbf{k}, \eta) = -2\pi \int_{-1}^1 d\alpha P_l(\alpha) \int_{\eta_{\text{dec}}}^{\eta_0} \frac{1}{6} \left[\mu'(\mathbf{k}, \tilde{\eta}) e^{i\alpha k(\eta_0 - \tilde{\eta})} + (1 - 3\alpha^2) \lambda'(\mathbf{k}, \tilde{\eta}) e^{i\alpha k(\eta_0 - \tilde{\eta})} \right] d\tilde{\eta}. \quad (\text{C78})$$

which, using equations (A34) and (A35), can be written as

$$\Delta_l(\mathbf{k}, \eta) = -(-i)^l \frac{2\pi}{3} \int_{\eta_{\text{dec}}}^{\eta_0} \left[\mu'(\mathbf{k}, \tilde{\eta}) j_l(k(\eta_0 - \tilde{\eta})) + \lambda'(\mathbf{k}, \tilde{\eta}) \mathcal{F}_l(k(\eta_0 - \tilde{\eta})) \right] d\tilde{\eta}. \quad (\text{C79})$$

where $\mathcal{F}_l(k(\eta_0 - \tilde{\eta}))$ is defined in equation (A35). We use this in equation (C77) to calculate the rms quadrupole $Q_{rms} = \sqrt{5C_2/4\pi}$ which we use to normalize the power spectrum.

D. The Numerical Scheme and its Accuracy

To follow the evolution of the background universe we have numerically solved equation (A3) for $a(\eta)$, along with equation (A40) for $\psi(q, \eta)$ for a set of values of q , and equation (A56) for $\omega_R(\eta)$. The q values have been chosen so that they are appropriate for the Gauss-Laguerre quadrature scheme, and we have used this method to evaluate the q integral required to evaluate $\omega_d(\eta)$ (equation (A42)) and the right hand side of equation (A56) at each time step. We have used 10 points to evaluate the q integrals and we find that there is no significant improvement if we increase the number of points. We have used an adaptive step-size fifth order Runge-Kutta subroutine ‘odeint’ (Press et. al. 1992) to follow the time evolution of the set of coupled ordinary differential equations. Along with the above mentioned quantities we have also evolved the quantities $\tau(q, \eta)$ and $\frac{\partial}{\partial q} \psi(q, \eta)$ which are required to follow the perturbations. The intermediate values of all these quantities are stored. We fit them with a cubic spline and use the intermediate values in studying the evolution of the perturbation.

The time-steps have been chosen so as to achieve a relative accuracy of 10^{-4} . For all the models the background universe is first evolved using $\Omega_{\text{CDM}0} = 1$. It sometimes happens that present contribution from the decay products is quite large and the total Ω_0 becomes greater than one. In such cases we reduce the value of $\Omega_{\text{CDM}0}$ and evolve the background again, and we keep on iterating the process until the value of Ω_0 converges to within 1 ± 0.001 .

For the metric perturbation we numerically solve the two second order differential equations (A10) and (A12) by converting them into four first order equations. These equations are solved together with equation (A15) for the CDM perturbations, and equations (A17) and (A18) for the perturbations in the photon-baryon fluid. This system of 7 differential equations is evolved using ‘odeint’ and the intermediate values of μ' and λ' at each time step are recorded and we fit these by a set of overlapping cubic polynomials and these are used in following the perturbations in the neutrinos. The metric perturbations are coupled to the perturbations in the neutrinos, and these have to be evaluated separately at each time step. For the massless neutrinos we numerically evaluate the integrals in equations (A36) and (A37) for every time step in ‘odeint’. Similarly, for the massive neutrinos we numerically evaluate the $\tilde{\eta}$ integrals in equations (A49), (A50), (A51) and (A53) for a set of values of q and we do the q integrals by a Gauss-Laguerre quadrature. For the decay products we have numerically evaluated the integrals in equations (A60) and (A61) at every time-step in ‘odeint’.

We have used 10 points for the q integrals, and we find that increasing the number of points does not significantly change the results for the feasible models in the range of k that we have considered.

The results of the computations described above yield the matter transfer function $T(k) \propto |\delta(\mathbf{k}, \eta_0)|^2$. We multiply this with k —the primordial Harrison Zel’dovich spectrum to obtain the power spectrum. This is normalized using equations (C77) and (C79) which we use to calculate Q_{rms} .

In our analysis we have ignored the baryon density and we use $\Omega_B = 0$. In addition, when following the evolution of the dark matter perturbations we have treated the photons as being tightly coupled to baryons until the present epoch. Finally, we have altogether ignored the interaction of the photons with the electrons and baryons when calculating the CMBR anisotropy. All these assumptions cause a few percent error in our results. These effects have been studied in detail for several models (see for instance Bond 1996), and it is found that the effect of baryons can be included by scaling the value of Γ as $\Gamma \times \exp(-2\Omega_B)$. Primordial nucleosynthesis imposes the restriction $\Omega_B h^2 \simeq 0.01$, and for $h = 0.5$ one expects a 8% error if the baryons are left out.

Treating photons as tightly coupled to baryons causes the sub-horizon scales perturbations in photons to continue to oscillate with the same amplitude even after recombination. In reality, once the photons decouple from the baryons their mean free path becomes comparable to the size of the horizon and sub-horizon perturbations in the photons start getting wiped out as a result of the free-streaming. However, the photons decouple in the matter dominated era where they play

no role in the dynamics of the dark matter perturbations, and these effects are negligible.

To check the accuracy of our numerical code we have compared our transfer function for several models with the runs of COSMICS (Bertschinger and Bode 1995) in the limit $\Omega_B \rightarrow 0$. For CDM models we get an agreement to better than 5% for $k \lesssim 1 \text{ Mpc}^{-1}$. A comparison of the transfer functions for various HDM and HCDM models allows us to test the reliability of our treatment of the massive neutrinos and we find that for the HDM model, in the range $k < 3 \text{ Mpc}^{-1}$ our transfer function differs from the transfer function calculated using COSMICS by less than 2%, which indicates that much of the error in our analysis come from the assumption of tight coupling. This results in larger errors in HCDM models, for which, in the range $0.1 \text{ Mpc}^{-1} < k \leq 1 \text{ Mpc}^{-1}$, the error is within 10%.

We have not pinpointed the exact cause of this discrepancy, but some of the possible sources are discussed below. One possible source of the error could be the fact that in dealing with the massive neutrinos one has to consider the evolution of neutrinos with different momentum separately and then integrate over the momentum. We have used only 10 values of momentum and the integration was done using a Gauss-Laguerre quadrature where a few of the points come with very low weights. COSMICS performs this integration using 8th-order Newton-Cotes method with as many as 128 points. This is one of the sources of the error and it may be possible to overcome this by using some other quadrature scheme (eg. Bond & Szalay, 1983) and by using more points. We have tried doubling the number of points but it does not make a very big difference in the results in the range $k < 0.5 \text{ Mpc}^{-1}$. Another possible cause for difference could be the fact that we have done all numerical integrations at a relative accuracy of 10^{-4} as compared to the relative accuracy of 10^{-8} in COSMICS. A point to be noted is that COSMICS uses various moments of the collisionless Boltzmann equation in order to follow the evolution of the perturbation in the neutrinos, and this involves a truncation which is externally enforced. Our method does not involve such a truncation as we use the analytic solution of the collisionless Boltzmann equation which is based on the method of characteristics, but it has an extra cost as we have to do an integration over the entire past at every time step. Our treatment also has another added advantage in that it involves only differential equations, and does not involve any algebraic equations, and we would expect it to be more stable compared to methods based on a combination of algebraic and differential equations. A little experimentation with the initial conditions shows that when they are set arbitrarily (i.e. a mixture of the growing and decaying modes) the solution goes over to the growing mode as expected and the effects of the decaying mode die away, showing that our numerical scheme is indeed stable and does not dependent critically upon any fine tuning of the initial conditions.

Finally we note that a 10% inaccuracy is acceptable in calculating the matter transfer function as it is well below the observational uncertainties. More accurate computations of decaying neutrino transfer functions may be required in the future as observations become more accurate. Also, a more intensive treatment of the massive neutrinos is required at smaller scales which will be essential to address issues related to galaxy formation in the decaying neutrino

models. A need for more accurate computing will also arise when computing CMBR anisotropies for comparing with proposed future observations at small angular scales. Work is currently in progress at improving the present numerical scheme so as to be able to address these questions.

REFERENCES

- Bardeen, J. M., Bond, J. R., & Efstathiou 1987, ApJ, 321, 28
- Bardeen, J. M., Bond, J. R., Kaiser, N., & Szalay, A. S. 1986, ApJ, 304, 15
- Baugh, C. M. & Efstathiou, G. 1994, MNRAS, 267, 32
- Bennett, C. L., et al. 1996, ApJ, 464, L1
- Bertschinger, E., Dekel, A., Faber, S. M., Dressler, A. & Burstein, D. 1990, ApJ, 364, 370
- Bertschinger, E. et. al. 1990, ApJ, 364, 370
- Bertschinger, E. & Bode, P. 1995, <http://arcturus.mit.edu/cosmics/>
- Bond, J. R. & Myers, S. 1996 ApJS, 103, 63
- Bond, J. R. 1996, Observations of Large-Scale Structure in the universe, Ed. Schaeffer, R., Les Houches Lecture Notes, To be published, Elsevier Science Publishers
- Bond, J. R. & Efstathiou, G. 1991, Phys. Lett. B, 265, 245
- Bond, J. R. & Szalay, A. S. 1983, ApJ, 276, 443
- Borgani, S., Gardini, A., Girardi, M., Gottloeber, S. 1997, astro-ph/9702154
- Bunn E. F. & White M. 1996, astro-ph/9607060
- Carlberg, R. G. et al. 1997, astro-ph/9704060
- Courteau, S., Faber, S. M., Dressler, A. & Willick, J. A. 1993, ApJ, 412, L51
- Dekel, A. 1994, Ann. Rev. Astron. Astroph. 32, 371
- Eke, V. R., Cole, S. & Frenk, C. S. 1996, MNRAS, 282, 263
- Efstathiou, G. 1992, MNRAS, 256, 43
- Efstathiou, G., Bond, J. R. & White, S. D. M. 1992, MNRAS, 258, 1p
- Efstathiou G., Sutherland W. J. & Maddox S. J. 1990, Nature, 348,705
- Evrard, A. E. 1989, ApJ, 341, L71
- Fukugita, M., & Yanagida, T. 1994, in *Physics and Astrophysics of Neutrinos* eds. M. Fukugita and A. Suzuki (Springer-Verlag)
- Gelb, J. & Bertschinger, E. 1994, ApJ, 436, 491
- Gelmini, G., Nussinov, S. & Peccei, R., 1992, Int. Jour. Mod. Phys. A, 7 ,3141
- Giallongo, E., et al. 1994, ApJ, 425, L1

- Giroux, M. L., & Shapiro, P. 1996, *ApJS*, 102, 191
- Henry, J. P. & Arnaud, K. A. 1991, *ApJ*, 372, 410
- Hu, W. & Sugiyama, N. 1996, *ApJ*, 471, 542
- Klypin, A., Holtzman, J., Primack, J. & Regös, E. 1993, *ApJ*, 416, 1
- Kofman, L., Gnedin, N. & Bahcall, N. 1993, *ApJ*, 413, 1
- Kofman L. & Starobinsky A. A. 1985, *Sov. Astron. Lett.*, 11, 27
- Kolb, E.W. & Turner, M.S. 1990, *The Early Universe* (Addison-Wesley, Redwood City, CA)
- Lanzetta, K. M., Wolfe, A. M., Turnshek, D. A. 1995, *ApJ*, 440, 435
- Liddle, A. R. & Lyth, D. H. 1993, *Phys. Rep.*, 231, 1
- Liddle, A. R., Lyth, D. H., Viana, P. T. P., White, M. 1996a, *MNRAS*, 282, 28
- Liddle, A. R., Lyth, D. H., Roberts, D. Viana, P. P. T 1996b, *MNRAS*, 278, 644
- Lin, H., Kirshner, R. P., Sheckman, S. A., Landy, S. D., Oemler, A., Tucker, D. J. & Schechter, P. A. 1996, *ApJ*, 471, 617
- Ma, C. & Bertschinger, E. 1994, *ApJ*, 434, L5
- Madau, P., Ferguson, H. C., Dickinson, M. E., Giavalisco, M., Steidel, C. C., & Fruchter, A. 1996, *MNRAS*, 283, 1388
- McNally, S. J. & Peacock, J. A. 1996, *MNRAS*, 277, 143
- Miralda-Escudé, J. & Ostriker, J.P. 1990, *ApJ*, 350, 1
- Mo, H. J. & Fukugita, M., 1996, *ApJ*, 467, L9
- Mo, H. J. & Miralda-Escudé, J., 1994, *ApJ*, 430, L25
- Netterfield, C. B., Devlin, M. J., Jarolik, N., Page, L., Wollack, E. J. 1997, *ApJ*, 474, 47
- Peacock, J. & Dodds, S., 1994, *MNRAS*, 267, 1020
- Peacock, J. A. & Dodds, S. J. 1996, *MNRAS*, 280, 19
- Pen, U. -L. 1996, *astro-ph/9610147*
- Press, W. H. & Schechter, P. 1974, *ApJ*, 187, 425
- Press, W. H., Teukolsky, S. A., Vetterling, W. T. & Flannery, B. P. 1992, *Numerical Recipes in C*, (Cambridge: Cambridge University Press)
- Sachs, R. K. & Wolfe, A. M., 1967, *ApJ*, 147, 73
- Sciama, D.W.1990, *Phys. Rev. Lett.*, 65, 2839
- Sciama, D.W. 1994, *Modern Cosmology and the Dark Matter Problem*, (Cambridge University Press)
- Sethi, S. K., 1997, *ApJ*, 474, 13

- Sethi, S. K. & Nath, B. B. 1996, MNRAS, in press.
- Smoot, G., et al., 1992, ApJ, 396, L1
- Steidel, C. C., Giavalisco, M., Pettini, M., Dickinson, M. & K.L. Adelberger, 1996, ApJ, 462, L17
- Storrie-Lombardi, L. J., McMahon, R. G., Irwin, M. J., Hazard, C. 1995, in *QSO Absorption Lines*, ESO Astrophysics Symposia ed. G. Meylan (Heidelberg: Springer)
- Strauss, M. A. & Willick, J. A., 1995, Phys. Rep., 261, 271
- Stompor R., Górski, K. M., Banday, A. J. 1995, MNRAS, 277, 1225
- Subramanian, K. & Padmanabhan, T., 1994, iucaa preprint-5/94
- Sugiyama, N. & Gouda, N., 1992, Prog. Theor. Phys., 88, 803
- Viana, P. T. P. & Liddle, A. 1996, MNRAS, 281, 323
- White, S. D. M., Efstathiou, G. & Frenk, C. S., 1993, MNRAS, 262, 1023
- White, M., Gelmini, G. & Silk, J. 1995, Phys. Rev D, 51, 2669
- Wolfe, A. M., Turnshek, D. A., Smith, H. E., Cohen, R. D. 1992, ApJ, 385, 151
- Yamamoto, K. & Bunn, E. F. 1996, ApJ, 464, 8

Fig. 1.— The contribution to $\omega(\eta)$ from the various components is shown as a function of the mode $k = \pi/(c\eta)$ which enters the horizon at the epoch η .

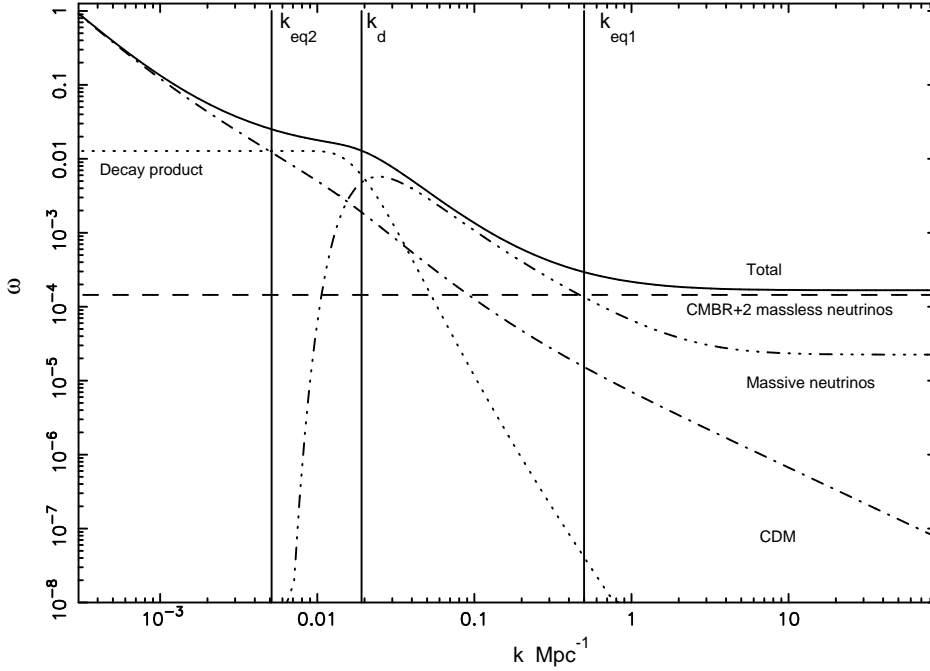


Fig. 2.— The solid curves show the transfer function for a decaying neutrino model with $h = 0.5$, $m_\nu = 200 \text{ eV}$ and $t_d = 10^{13} \text{ s}$. The smooth curve is the result of the numerical computation whereas the jagged curve is based on the crude approximation to the transfer function discussed in section 2. The dashed curve shows the transfer function for the $h = 0.5$ CDM model.

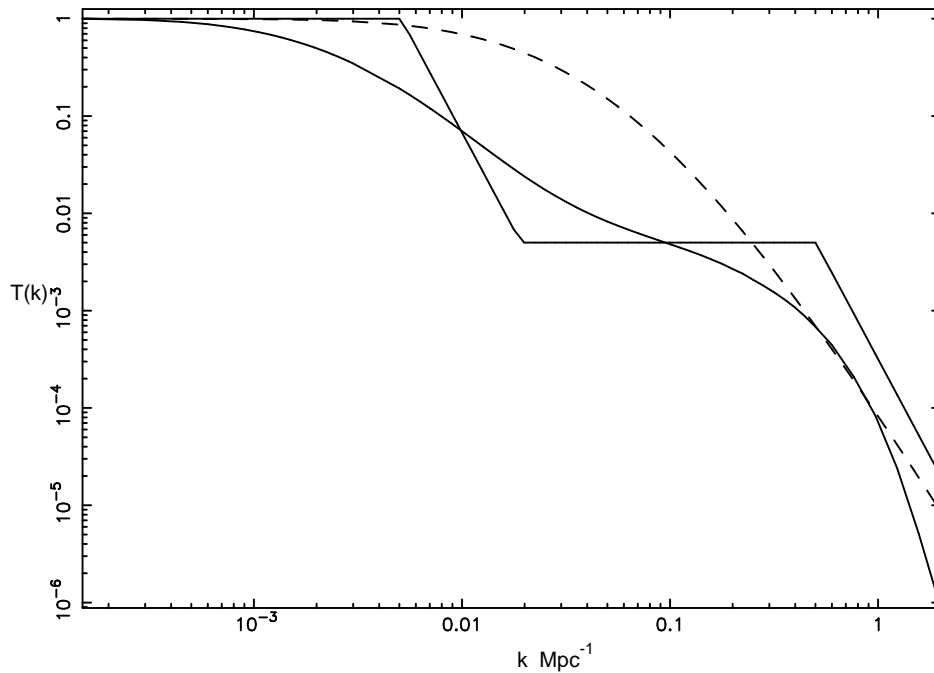


Fig. 3.— This shows the power spectra for several decaying neutrino models all obtained by varying m and t_d keeping $m_\nu^2 t_d$ a constant. The CDM power spectrum is shown for comparison. Also shown is the APM power spectrum (filled squares) and the best fit to the LCRS power spectrum (dashed-dotted thick curve). $b = 1.2$ has been assumed in plotting the APM and LCRS power spectra and $h = 0.5$ is used for all the power spectra shown here.

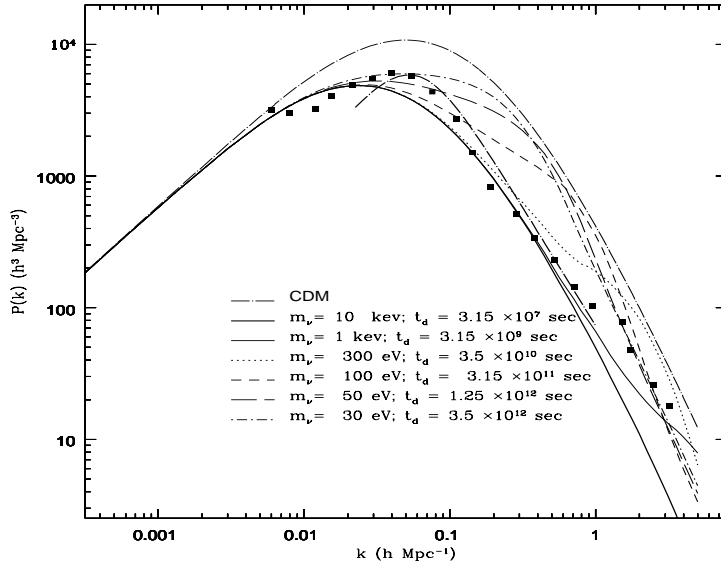


Fig. 4.— This shows how σ_R (R in h^{-1} Mpc) changes as a function of m_ν for a class of models for which $m_\nu^2(\text{keV})t_d(\text{yr}) = 100$. The corresponding values for the standard CDM model are: $\sigma_8 = 1.26$, $\sigma_4 = 2.32$, $\sigma_1 = 3.81$, $\sigma_{0.5} = 5.75$, and $\sigma_{0.25} = 10.89$.

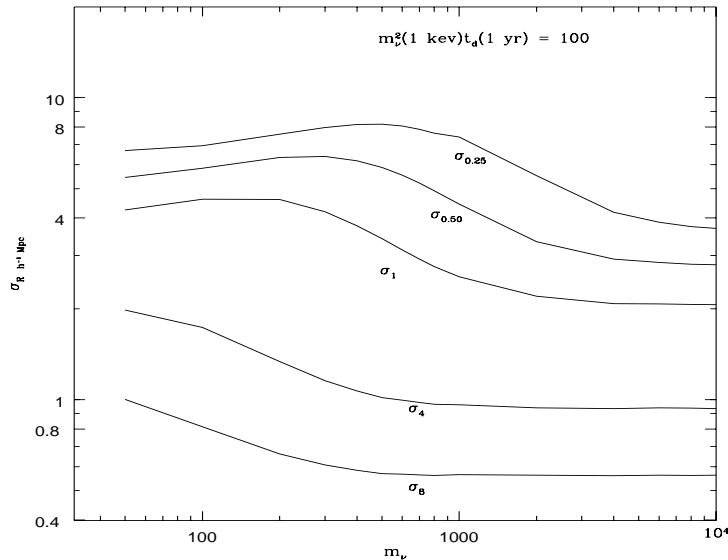


Fig. 5.— This shows the power spectrum for several models which give acceptable value of σ_8 (Table 1). Most of these models are ruled out on comparison to the APM and LCRS power spectra which have been plotted here for $b = 1.2$. These models also fail to make reasonable predictions for the peculiar velocities (Table 1). $h=.5$ has been used here.

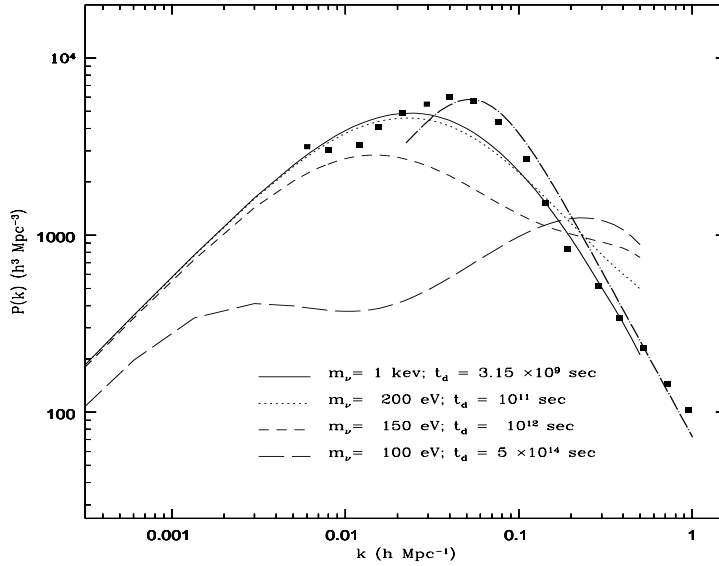


Fig. 6.— Here we show the *r.m.s.* bulk velocity in spheres of radius R after smoothing with a Gaussian of $12h^{-1}$ Mpc. This is plotted as a function of R for the following decaying neutrino models, all of which use $h = .5$: (1) $m_\nu = 1$ keV, $t_d = 3.15 \times 10^9$ sec (*solid curve*), (2) $m_\nu = 200$ eV, $t_d = 10^{11}$ sec (*dotted curve*), (3) $m_\nu = 150$ eV, $t_d = 10^{12}$ sec (*short dashed curve*), and (4) $m_\nu = 100$ eV, $t_d = 5 \times 10^{14}$ sec (*long dashed curve*). The data points shown, $V_{40} = 388 \pm 67$ km/sec and $V_{60} = 327 \pm 88$, are taken from Bertschinger et al. (1990)

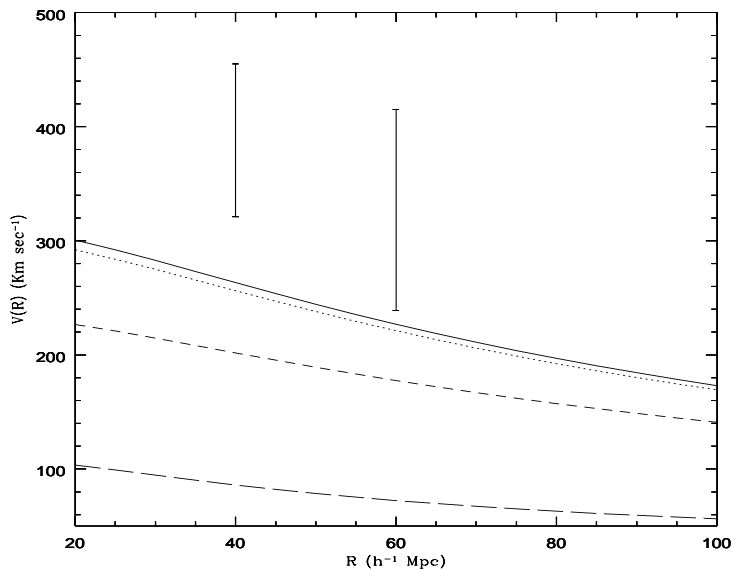


Fig. 7.— Here we show the power spectrum for some of the radiatively decaying neutrino models (where a small fraction of neutrinos $B \simeq 10^{-5}$ – 10^{-7} decay into photons) which satisfy various observations of the ionization of the intergalactic medium at high redshifts.

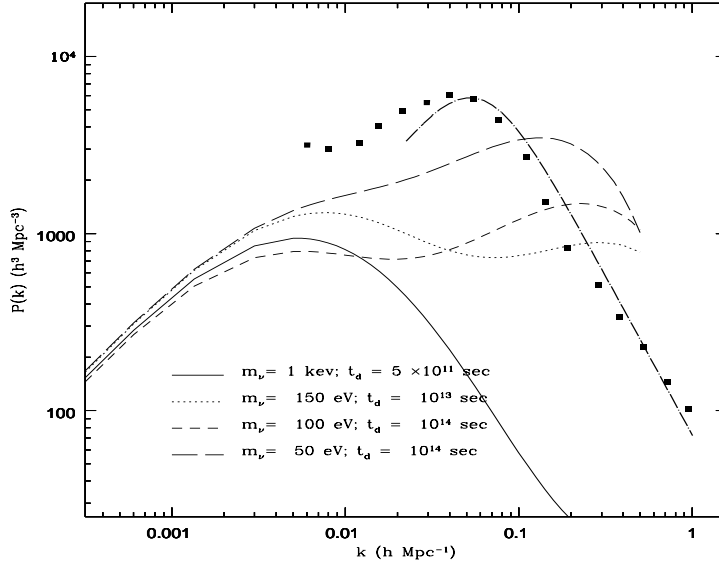


Fig. 8.— The parameter space allowed by structure formation bounds (*shaded region*) corresponding to $0.2 \leq \Gamma \leq 0.3$ where $\Gamma(m_\nu, t_d)$ is given by Eq. (14) is shown along with the region on the m_ν – t_d plane allowed by IGM considerations (i.e. Eqs. (15) and (16)) (*hatched region*).

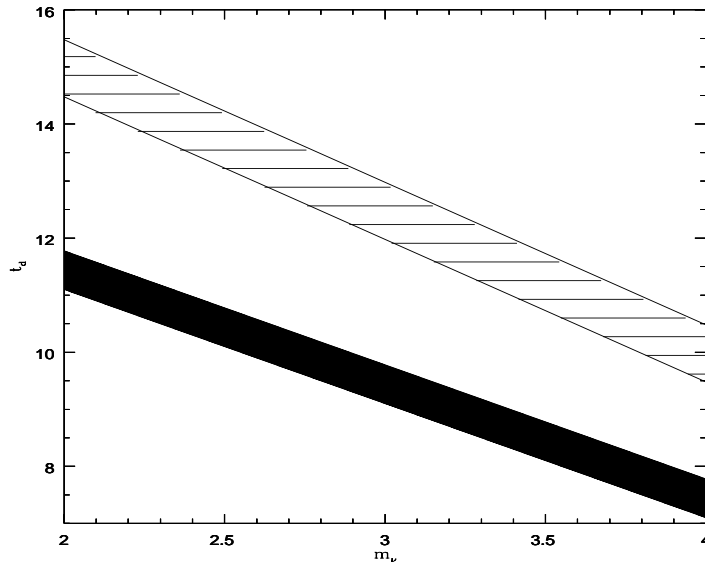


Fig. 9.— The density of collapsed baryons Ω_{col} for several structure formation models is compared to the density of neutral hydrogen Ω_{HI} observed in the damped Lyman- α clouds. The shaded region corresponds to Eq. (17) (Lanzetta, Wolfe, and Turnshek 1995). The data point at $z \simeq 4$ is taken from Storrie-Lombardi et al. (1995).

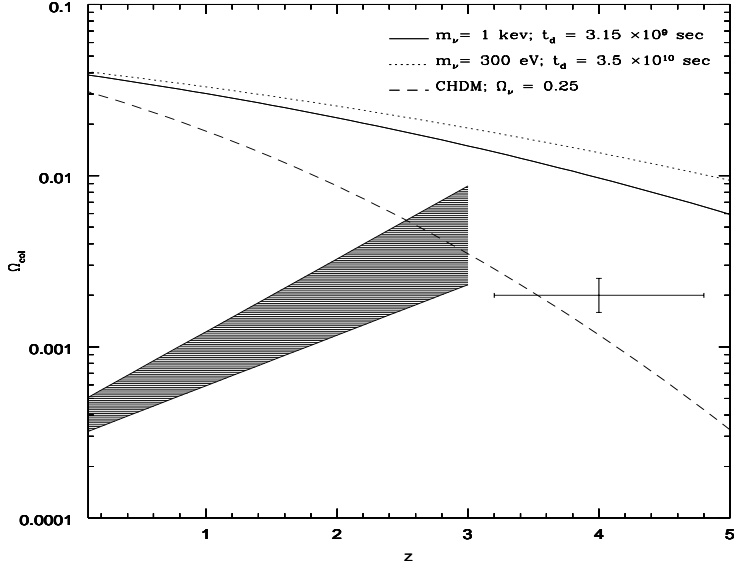


Table 1: Values of σ_8 and *r.m.s.* bulk velocity in km/s in spheres of radius $40h^{-1}$ Mpc and $60h^{-1}$ Mpc after smoothing with a Gaussian of $12h^{-1}$ Mpc.

m_ν (eV)	t_d (sec)	σ_8	V_{40}	V_{60}
10^4	3.15×10^7	0.55	263	226
10^3	3.15×10^7	1.13	345	286
10^3	3.15×10^9	0.56	263	226
10^3	5×10^{11}	0.1	95	88
500	1.26×10^{10}	0.57	262	226
300	3.5×10^{10}	0.6	263	226
150	1.4×10^{11}	0.71	264	226
150	10^{12}	0.62	201	177
150	10^{13}	0.58	132	118
100	3.15×10^{11}	0.81	266	228
100	10^{14}	0.72	113	98
100	5×10^{14}	0.69	86	72
50	1.25×10^{12}	1.0	274	232
50	10^{14}	0.98	182	153
30	3.5×10^{12}	1.08	285	239